CONDITIONS FOR FORCED AND SUBHARMONIC OSCILLATIONS IN RELAY AND QUANTIZED FEEDBACK SYSTEMS

LIM LI HONG IDRIS

NATIONAL UNIVERSITY OF SINGAPORE

2009

CONDITIONS FOR FORCED AND SUBHARMONIC OSCILLATIONS IN RELAY AND QUANTIZED FEEDBACK SYSTEMS

LIM LI HONG IDRIS

(B.Eng., NUS)

A THESIS SUBMITTED

FOR THE DEGREE OF DOCTOR OF PHILOSOPHY

DEPARTMENT OF ELECTRICAL
AND COMPUTER ENGINEERING

NATIONAL UNIVERSITY OF SINGAPORE

2009

Acknowledgments

I would like to express my deepest gratitude to my supervisor, Prof. Loh Ai Poh, who has not only given me a lot of support and guidance on my research, but also cared about my life throughout my Ph.D. study. Without her gracious encouragement and generous guidance, I would not be able to finish the work so smoothly. Her wealth of knowledge and accurate foresight have greatly impressed and benefited me. I am indebted to her for her care and advice in my academic research and other personal aspects.

I would like to extend special thanks to Prof. Derek P Atherton of University of Sussex, Prof. Wang Qing Guo and Dr Lum Kai Yew, for their comments, advice and the inspiration given, which have played a very important role in this piece of work.

Special gratitude goes to Prof. Wang Qing Guo, Dr Lum Kai Yew, Prof. Shuzhi Sam Ge, Prof. Ben M Chen, Prof. Xu Jian-Xin, Dr Arthur Tay, Prof. Vivian Ng and Dr. Xiang Cheng who have taught me in class and/or given me their kind help in one way or another.

Not forgetting my friends and colleagues, I would like to express my thanks

to My Wang Lan, Mr Lu Jingfang, Miss Huang Ying, Mr. Wu Dongrui, Mr. Wu Xiaodong, Ms. Hu Ni, Ms Wang Yuheng, Mr Shao Lichun, Miss Gao Hanqiao, Mdm S. Mainavathi and Mdm Marsita Sairan and many others in the Advanced Control Technology Lab (Center for Intelligent Control) for making the everyday work so enjoyable. I greatly enjoyed the time spent with them. I am also grateful to the National University of Singapore for the research scholarship.

Finally, this thesis would not have been possible without the love, patience and support from my family. The encouragement from them has been invaluable. I would like to dedicate this thesis to them and hope that they will find joy in this humble achievement.

Lim Li Hong Idris

March, 2008

Contents

Acknowledgments **ii**

Summary **vii**

List of Tables **ix**

List of Figures **x**

List of Symbols **xiii**

1 Introduction **1**

1.1 Motivation 1

1.2 Contributions 10

1.3 Organization of the Thesis 12

2 Forced and Subharmonic Oscillations under Relay Feedback **13**

2.1 Introduction 13

2.2 Problem Formulation 14

2.3 Conditions for Periodic Switching 18

2.3.1 Determination of $R_{\min 1}$ and $R_{\min 2}$ 20

2.3.2 Frequency Ranges of External Signal for SO 27
2.4 Limits of ν in SO 32
2.4.1 SO analysis for first order plants 32
2.4.2 SO analysis for higher order plants 35
2.5 Conclusion 39

3 Design of Amplitude Reduction Dithers in Relay Feedback Systems 42

3.1 Introduction 42
3.2 Problem Formulation 43
3.3 Identification of T_f^* 46
3.4 Solution of T_f^* using the Generalized Tsypkin Locus 50
3.5 Special Cases 52
3.6 Quenching with Other Dither Signals 58
3.7 Applications 60
3.8 Conclusion 64

4 Limit Cycles in Quantized Feedback Systems under High Quantization Resolution 66

4.1 Introduction 66
4.2 Problem Formulation 68
4.3 Analysis 71
4.3.1 Limit Cycles 71
4.3.2 Stability of Limit Cycles 75

4.3.3 Special Cases 81

4.4 Conclusions 86

5 Conclusions **90**

5.1 Main Findings 90

5.2 Suggestions for Further Work 92

Author's Publications **94**

Bibliography **96**

Summary

This thesis contributes to control literature in the following three topics: (1) Forced and subharmonic oscillation in relay feedback systems, (2) Design of sinusoidal dither in relay feedback systems, and (3) Limit cycles in quantized feedback systems.

Forced oscillations is a phenomenon where the external signal causes oscillations of the same frequency to occur in the system. The necessary and sufficient conditions for forced and subharmonic oscillations (FO and SO, respectively) in an externally driven single loop relay feedback system (RFS) are analyzed. It is shown that FO of any frequency will always occur in the RFS if and only if the amplitude of the external forcing signal is larger than some minimum. This minimum amplitude is determined by graphical/numerical approaches. In contrast, the existence of SO is dependent on both the amplitude and frequency of the external signal. Interestingly, one may not be able to obtain any SO for arbitrary frequencies even if the amplitude of the external signal is large. Given this important fundamental difference, the range of frequencies where SO can exists is also determined, along with the necessary minimum amplitude of the external signal required for the SO

to occur.

The use of dithers to achieve signal stabilization and quenching of limit cycles is well known in nonlinear systems. The idea is similar to the phenomenon of forced oscillations (FO). This idea is used to design a dither signal which results in reduced oscillation amplitudes. The minimum dither frequency, f_{min}, which satisfies this amplitude reduction specification is determined. f_{min}, is also shown to be independent of the dither shape. The design of an optimal sinusoid with the least amplitude is also presented. Analytical expressions for f_{min} are obtained for first and second order plants. For higher order systems, the identification of f_{min} using the Tsypkin loci is shown.

In the last part of this thesis, a more general nonlinearity (the quantizer) in a feedback system is studied. It is well known that a quantized feedback system can be stabilised by increasing the resolution of the quantizer. However, limit cycles have also been found under certain conditions at high resolution. These necessary and sufficient conditions for the existence of limit cycles are examined. Solutions for the limit cycle period and switching instants obtained via the inverse-free Newton's method are used to assess the stability of the limit cycle under high resolution with the Poincaré map. The stability of the limit cycle can be identified by evaluating the magnitude of eigenvalues of the Jacobian of the Poincaré map. Analytical results on the existence of limit cycles in first systems are presented. The bounds on the quantization resolution for stable limit cycles in a second order system are also identified.

List of Tables

2.1 Table of R and $R_{\nu,min}$ for example 2.6. 38

List of Figures

1.1 Single loop with external forcing signal. 4

1.2 Amplitudes due to FO and SO are lower than that of self oscillation. 4

1.3 (a) SO of $\nu = 7$ obtained with $\theta = 3.7726$. (b) SO of $\nu = 9$ obtained with $\theta = 0$. 5

2.1 Single loop with external forcing signal. 15

2.2 Illustration of switching plane. 16

2.3 Different oscillations in an externally driven RFS. 17

2.4 Illustration of θ on the complex plane. 24

2.5 Tsypkin locus for a second order plant. 27

2.6 R_{min} comparison for plant in (2.34). 27

2.7 Dependence of SO on R and $T/2$. 30

2.8 Example where the desired SO with $\nu = 3$ is obtained. 31

2.9 Different νs obtained with a fixed R and varying $T/2$. 32

2.10 Plot of the bounds for example 2.3, 'o': Calculated, '□':Simulated. . 35

2.11 Plot of the bounds for example 2.4, 'o': Calculated, '□':Simulated. . 36

2.12 Plot of the bounds for example 2.5, 'o': Calculated, '□':Simulated. . 36

2.13 Plot of bounds for example 2.6, 'o': Calculated, '□':Simulated. . . . 37

2.14 Multiple νs of SO observed for example 2.6 with varying R. 37

2.15 Effect of only varying R for example 2.7, 'o': Calculated bounds, '□':Simulated bounds. 39

2.16 (a) SO of $\nu = 3$ obtained with $\theta = 4.6783$. (b) SO of $\nu = 5$ obtained with $\theta = 0$. 40

2.17 Effect of varying R, z_0 and θ for example 2.7, 'o': Calculated bounds, '□':Simulated bounds. 40

2.18 Effect of the initial condition for example 2.7. 41

3.1 RFS with external forcing signal. 44

3.2 Plot of the amplitude of oscillation against $T_f/2$ for $G(s) = 1000/(s^5 + 6s^4 + 58s^3 + 211s^2 + 629s + 471)$. 47

3.3 Plot of the amplitude of oscillation against $T_f/2$ for $G(s) = \frac{1}{s^2+2s+20}$. 48

3.4 Plot of the generalized Tsypkin Locus in example 3.1. 51

3.5 Self oscillation and FO of differing $T_f/2$ in example 3.2. 54

3.6 Plot of the amplitude of oscillation against $T_f/2$ in example 3.2. . . 55

3.7 (a)Plot of the Tsypkin Locus in example 3.3. (b)Plot of the amplitude of oscillation against $T_f/2$ in example 3.3. 57

3.8 (a)Plot of the Tsypkin Locus in example 3.4. (b)Plot of the amplitude of oscillation against $T_f/2$ in example 3.4. 59

3.9 (a) Maximum oscillation amplitudes with triangular dithers. (b) Plot of $u(t)$, $c(t)$ and $f(t)$ for $T_f/2 = 0.7207$. 60

3.10 (a)Maximum oscillation amplitudes with composite sinusoidal dithers. (b)Plot of $u(t)$, $c(t)$ and $f(t)$ for $T_f/2 = 0.7207$. 61

3.11 Block diagram of the Missile Roll-Control problem. 62

3.12 (a)Comparison of the oscillation amplitudes in example 3.5. (b)Comparison of the steady state oscillation amplitudes in example 3.5. 62

3.13 Plot of $c(t)$ with sinusoidal and sawtooth dithers. 63

3.14 Model of the DC motor in example 3.6. 64

3.15 Comparison of the oscillation amplitudes of the DC motor in example 3.6. 65

3.16 Comparison of the oscillation amplitudes between the sinusoidal and sawtooth dithers in example 3.6. 65

4.1 Quantized feedback system. 69

4.2 5-level limit cycle. 71

4.3 3-level limit cycle. 74

4.4 2 step limit cycle with $\Delta = 2.5$. 80

4.5 States of 2 step limit cycle with $\Delta = 2.5$. 87

4.6 2 step limit cycle with $\Delta = 0.25$. 87

4.7 2 step limit cycle with $\Delta = 0.05$. 88

4.8 States of 2 step limit cycle with $\Delta = 0.05$. 88

4.9 (a) 1 step limit cycle with $\Delta = 0.0005$. (b)States of 1 step limit cycle with $\Delta = 0.0005$. 89

List of Symbols

R	External forcing signal amplitude
$f(t)$	External forcing signal
ν	Subharmonic order
θ	Phase of external forcing signal
f_{min}	Dither frequency lower bound
T_f*	Upper bound on dither period
T_f	External forcing frequency
$G(s)$	Transfer function of linear system
$\mathbf{A}$	State Matrix
$\mathbf{B}$	Input Matrix
$\mathbf{C}$	Output Matrix
L	Time delay
$u(t)$	Input vector
$c(t)$	Output vector
h	Relay height
y	RFS output

Σ_L	RFS system
$F(t)$	Switching plane
t_0	Time after steady state switching
ω_f	External forcing frequency
$z(t)$	State vector
K_c	Critical gain of linear element
$\Lambda(.)$	Tsypkin Locus
R_{min}	Minimum amplitude required
Ω	Frequency ranges for SO
$R_{\nu,min}$	Minimum amplitude for SO of order ν
n	Parameterisation of L w.r.t. T_f
λ_i	Roots of the plant
a	Real part of complex roots
b	Imaginary part of complex roots
R_a	Armature resistance of motor
L_a	Inductance of motor
J	Mechanical resistance
β	Viscous coefficient
θ_a	Angular position of shaft
i_a	Armature current
k_t	torque constant
M	Saturation limit of quantizer

δ	Step size of quantizer
Q_δ	Quantizer
k	Number of quantization levels
τ_i	Switching time instants
J	Definition of Jacobian of Poincaré map
z_m^0	State at m-th switching point
W	Jacobian of Poincaré map for quantizer

Chapter 1

Introduction

1.1 Motivation

The advent of automation in various fields of engineering encouraged the developments and applications of control theory. In the area of linear control, extensive results were developed. However, in many real life systems, nonlinearities are commonly present. Classical nonlinear control theory lays the foundation for many advanced studies in modern control today. Nevertheless, some problems remain open and their solutions are sought. In this thesis, some of these problems are studied. They are listed as follows.

A. Forced and Subharmonic Oscillations under Relay Feedback

Relay feedback as a control technique has received much attention since 1887 when Hawkins discovered that a temperature control system has a tendency to oscillate under discontinuous control. Continued attention on relay feedback was due to its widespread use in mechanical and electro-mechanical applications. Since

then, the study of the relay feedback system (RFS) has been spurred on by the modern developments in supervisory switched systems and variable structure controllers. The latest application of relay feedback is in the use of its limit cycling properties which are useful in controller tuning and identification (Bernardo and Johansson, 2001; Tsypkin, 1984; Lin *et al.*, 2002).

The application of the RFS in a wide range of settings has prompted extensive studies on its behaviour. Due to the switching nature of the relay, the RFS is essentially nonlinear and the output of the relay is discontinuous at its switching instants. Thus, the RFS naturally falls into the class of non-smooth systems whose study is well covered in (Filippov, 1988). The complex dynamics associated specifically with the relay results in various interesting phenomena such as the existence of fast switches, sliding motion and limit cycling. The existence of fast switches and sliding motion has been extensively studied in (Johansson *et al.*, 1999), (Bernardo and Johansson, 2001) and (Fridman, 2002) while some global stability results of limit cycles in the RFS were shown in (Goncalves *et al.*, 1999).

There is also substantial literature in the general area of non-smooth dynamical systems with external excitation. Two classical examples are (Feigin, 1970) and (Nordmark, 1991). Other works include (Feigin, 1974; Feigin, 1994; A. Gelig, 1998; Piccardi, 1994). Such externally forced RFS are also observed in multi-loop controller tuning, originally introduced by Astrom and Hagglund in 1984 (Åström K J, 1984) and later extended to multi-loop processes in (Loh *et al.*, 2000), wherein signals from one loop drives another loop and cause a change in the oscillation behaviours in the other loops. With the extension of the auto-tuning techniques to

multivariable systems, a better understanding of FO was given in (Lim *et al.*, 2005).

Our quest to study the externally driven RFS (see Figure 1.1) also has to do with the existence of other physical phenomena which includes self-excited oscillations. Such self oscillations disturb the normal operation of the system and cause increased wear and tear of system elements. In some cases, the stress created by the self oscillations can be reduced by inducing FO or SO of lower amplitudes. Simulation studies were performed on the missile roll control system in (Taylor, 2000; Gibson, 1963). By inducing FO or SO of an appropriate frequency, smaller oscillations as compared to the system's self oscillations were obtained. For example, with an external sinusoidal signal of frequency $\omega = 84.9$ rad/s and amplitude $R = 0.1$ and 0.55, SO and FO were obtained respectively, as shown in Figure 1.2. The advantage is that the FO and SO amplitudes are much lower than that of the self-oscillations. In (Luigi Iannelli, 2003*a*; Luigi Iannelli, 2003*b*; Luigi Iannelli, 2006; Naumov, 1993; A. A. Pervozvanski, 2002; Mossaheb, 1983), damping of self-excited oscillations by external signals was also shown. All these applications motivate the need to identify exact conditions required to achieve FO and SO in an externally driven RFS.

There are many methods which attempt to predict the existence of oscillations in RFS. The most common approach being the describing functions. Time domain approaches are also presented in (Hamel, 1949; J.K.-C. Chung, 1966; Q.-G. Wang, 2003). Other methods by Tsypkin (Tsypkin, 1984) and Atherton (Atherton, 1982) attempted to identify the amplitude of the external forcing signal required for FO and SO. However, they did not present explicit minimum requirements on the

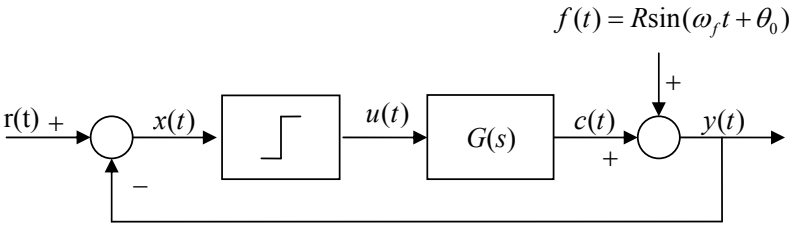

Fig. 1.1. Single loop with external forcing signal.

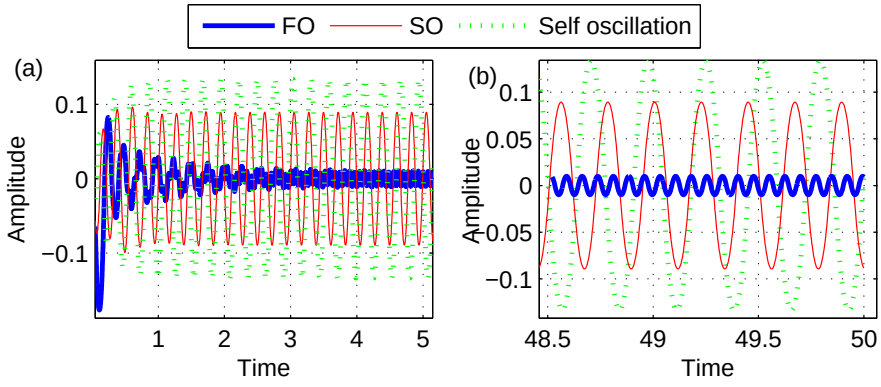

Fig. 1.2. Amplitudes due to FO and SO are lower than that of self oscillation.

external signal. Neither was there clear distinctions between FO and SO. Unlike FO, the prediction of SO is more difficult because they cannot be observed for all $f(t)$ of arbitrary frequencies and amplitudes. Furthermore, under small differences in conditions, the order of SO also changes. This problem is illustrated in Figure 1.3 where the order of SO changes from $\nu = 7$ to $\nu = 9$ when θ (which is the initial phase of $f(t)$) changes from 3.7726 rad to 0 rad with all other conditions unchanged.

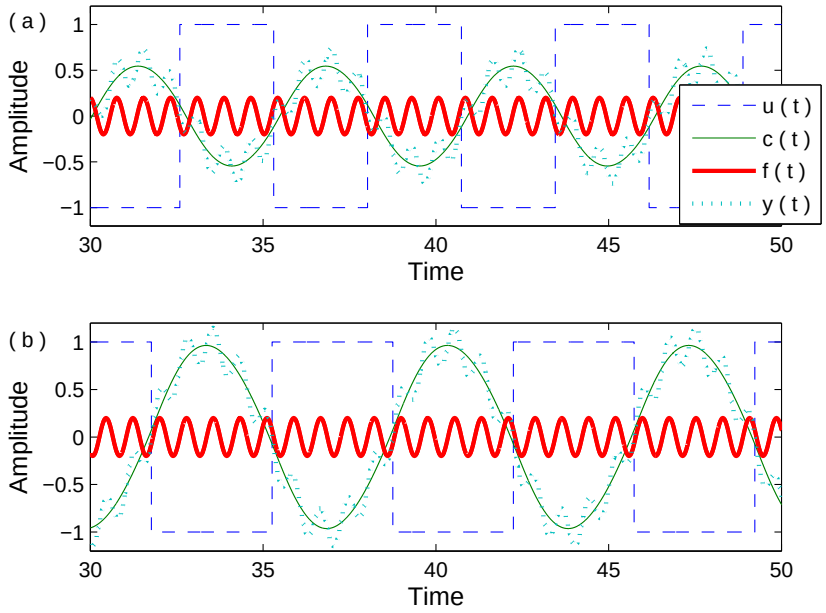

Fig. 1.3. (a) SO of $\nu = 7$ obtained with $\theta = 3.7726$. (b) SO of $\nu = 9$ obtained with $\theta = 0$.

In the thesis, the minimum conditions required for FO and SO to occur in a RFS are presented. As a result of the analysis, a fundamental difference between FO and SO was uncovered. In particular, we show that FO is always possible at any frequency if and only if certain minimum conditions on the external signal

are met. This, however, does not apply to SO. SO requires specific conditions involving the frequency and amplitude of the external signal. Further new results involving the orders of SO were also obtained from our analysis.

B. Design of Amplitude Reduction Dithers in Relay Feedback Systems

Switching is an important concept widely used to control certain behaviours in a system. In power electronics, for instance, switching is used effectively in the control of converters. The problem with switching, however, is that it causes great difficulties in the analysis of the behaviour in the overall nonlinear system, especially for discontinuous systems involving relays. For example, in the dithered RFS considered in Luigi Iannelli et al. (Luigi Iannelli, 2003*a*; Luigi Iannelli, 2003*b*), only an approximate analysis was proposed despite having a very specific dither signal. Their analysis led to a lower bound of the dither frequency which guarantees the stability of the nonsmooth system. The final bound was also shown to be conservative.

As pointed out in Pervozvanski and Canuda de Wit (A. A. Pervozvanski, 2002), rigorous analysis for dithered discontinuous system such as that of a dithered RFS cannot be achieved using conventional methods. The common approach is generally to approximate the original discontinuous dithered system with a smooth system. Stability can be proven for a sufficiently high dither frequency by the use of the classical averaging theory, formerly developed by Zames and Shneydor(Zames and Falb, 1968; G. Zames, 1977; G. Zames, 1976) for continuous nonlinear systems. Other related works can be found in Mossaheb(Mossaheb, 1983), Luigi Iannelli et

al.(Luigi Iannelli, 2006) and Lehman and Bass(Brad Lehman, 1996). Their results showed that a sufficiently high frequency dither can reduce the limit cycles in the dithered system to a negligible ripple but exact conditions on the dither periods and amplitudes were not given.

In our previous work on forced oscillation in RFS (Loh *et al.*, 2000; Lim *et al.*, 2005), we have given very specific conditions for the design of external sinusoidal dither signals that can induce oscillations of the same frequency as this dither signal. The analysis given was exact and does not rely on any approximation theory. The results were also necessary and sufficient. In this part of the thesis, we extend the results in (Loh *et al.*, 2000; Lim *et al.*, 2005) to design sinusoidal dither signals that will result in stable oscillations of arbitrarily low amplitudes. A lower bound on the dither frequency, f_{min}, (equivalently an upper bound, T_f^*, on the dither period) is first determined based on the response of the linear system to square wave inputs. For dithers with period $T_f < T_f^*$, the oscillation amplitudes in the RFS can be guaranteed to decrease monotonically with decreasing T_f. The amplitude of the sinusoidal dither signal can be designed based on the analysis in (Loh *et al.*, 2000; Lim *et al.*, 2005). This result is much stronger than other previous results because bounds obtained are tight and requires no approximation. It exploits the specific structure of the relay and the linear system, allowing exact responses to be written and analyzed.

Our analysis is also not limited to the sinusoidal dither. In fact, it applies to any periodic symmetric dither signals of other shapes. This is because as long as the dither amplitude is sufficiently large to induce forced oscillations of period T_f

in the system, the input to the plant is always a symmetric square wave due to the relay switchings. Thus the plant's steady state output is only dependent on the relay's switching period T_f and is independent of the actual shape of the dither signal. Therefore, the identification of the bound on the dither period in this paper can be applied to other dither shapes.

C. Limit Cycles in Quantized Feedback Systems under High Quantization Resolution

As early as 1956, Kalman studied the effect of quantization in a sampled data system and pointed out that the feedback system with a quantized controller would exhibit limit cycles and chaotic behaviour(Kalman, 1956; Toshimitsu U, 1983). Since then, many methods have been proposed to eliminate limit cycles in SISO and MIMO quantized feedback systems such as increasing the quantization resolution, dithering the quantizer with a DC signal and stabilising controllers design etc (Curry, 1970; R.K. Miller and Farrel, 1989; K, 1991; Juha Kauraniemi, 1996; J.D. Reiss, 2005; Delchamps, 1990; Fu and Xie, 2005). As compared to the other methods, the most direct method which is to increase the quantizer resolution, will be examined in this paper.

In the current literature, a standard assumption is that the quantizer parameters are fixed in advance and cannot be changed. However, in a real-life system like the digital camera, the resolution can be easily adjusted in real time(Liberzon, 2003). Hence, we adopt the approach that the quantizer resolution can be adjusted. In this paper, the problem structure we examine is the hybrid system, which is a continuous-time system with a uniform quantizer in feedback. The recent paper

(Brockett & Liberzon, 2000) shows that if a linear system can be stabilised by a linear feedback law, then it can also be globally asymptotically stabilised by a hybrid quantized feedback control policy.

Under high quantizer resolution, the uniform quantizer resembles a linear gain with many minute switches. Hence, if the continuous-time system is stable under negative closed loop feedback, the hybrid system is indeed expected to stabilise. In fact, many control methodologies derive stability by increasing the quantization resolution.(R.W. Brockett, 2000; Liberzon, 2003) However, in this paper, we present the existence of limit cycles under high quantizer resolution. There exist literature on the conditions required for limit cycles (Marcus Rubensson, 2000; Goncalves, 2005) but the problem under high resolution has not been examined, to the best of our knowledge. Thus, there is a need to study the behaviour of the system under high resolution in greater depth.

For the evaluation of the limit-cycle properties of the hybrid system, the inverse-free Newton's method is used(Y. Levin, 2003). As the inverse Jacobian for the hybrid system does not exist in many cases, the conventional Newton's method cannot be applied. Multiple solutions of the switching instants and period can be obtained with the inverse-free Newton's method, depending on the initial states of the system. Due to multiple discrete levels in the quantizer, it provides an additional degree of freedom for the limit-cycle characteristics. For instance, both a 1-step limit cycle and a 2-step limit cycle can be reached with different initial conditions in a hybrid system with a 40 step quantizer and the switching instants and the periods of each limit cycle can differ. Thus, the limit cycle solution is

non-unique, unlike the relay (1-step quantizer) feedback system. This additional degree of freedom can be reduced by fixing the number of levels expected in a limit cycle. If so, we are able to identify the limit cycle solution through the necessary conditions required. A further check on the stability of the limit cycle via the Poincaré map reveals the existence of the limit cycle in the system.

1.2 Contributions

In this thesis, new results in forced and subharmonic oscillations for relay feedback systems are given. The idea from forced oscillations is applied to design sinusoidal dither signals that will result in stable oscillations of arbitrarily low amplitudes. For a more general nonlinearity, the quantizer, the conditions for the existence and stability of limit cycles in quantized feedback systems under high quantization resolution are examined. Detailed contributions in each of these areas are given as follows:

A. Forced and Subharmonic Oscillations under Relay Feedback

The necessary and sufficient conditions for forced and subharmonic oscillations (FO and SO, respectively) in an externally driven single loop relay feedback system (RFS) are examined. It is shown that FO of any frequency will always occur in the RFS if and only if the amplitude of the external forcing signal is larger than some minimum. This minimum amplitude can be determined by graphical/numerical approaches. In contrast, the existence of SO is dependent on both the amplitude and frequency of the external signal. The main contribution of this thesis lies in the

discovery of this fundamental difference between FO and SO. FO is possible for any frequency of the external forcing signal as long as its amplitude was sufficiently large. This was however not the case for SO. A complex relationship between frequency, amplitude and ν exists for SO. Specifically, not all forcing signals can drive the RFS at any order ν even if the amplitude of the external signal is large. The ranges of frequencies where SO of certain orders can be obtained were derived. Results for FOPDT plants were completely given. Other behaviours for higher order plants were also presented.

B. Design of Amplitude Reduction Dithers in Relay Feedback Systems

The idea from the phenomenon of FO is used to design a dither signal which results in reduced oscillation amplitudes. The minimum dither frequency, f_{min}, which satisfies this amplitude reduction specification is determined. f_{min}, is also shown to be independent of the dither shape. Furthermore, if the dither is a sinusoid, the design of an optimal sinusoid with the least amplitude is presented. Analytical expressions for f_{min} are obtained for first and second order plants. For higher order systems, it is shown how the Tsypkin loci can be used to identify f_{min}. Two motivating examples on the missile roll control system and the control of a DC motor is presented.

C. Limit Cycles in Quantized Feedback Systems under High Quantization Resolution

For a more general nonlinearity (the quantizer), the existence of limit cycles under high quantizer resolution is examined. It is well known that a quantized

feedback system can be stabilised by increasing the resolution of the quantizer. However, limit cycles have also been found under certain conditions at high resolution. These necessary and sufficient conditions for the existence of limit cycles are examined. Solutions for the limit cycle period and switching instants obtained via the inverse-free Newton's method are used to assess the stability of the limit cycle under high resolution with the Poincaré map. The stability of the limit cycle can be identified by evaluating the magnitude of eigenvalues of the Jacobian of the Poincaré map. Analytical results on the existence of limit cycles in first systems are presented. The bounds on the quantization resolution for stable limit cycles in a second order system are also identified.

1.3 Organization of the Thesis

The thesis is organized as follows. Chapter 2 presents the results on the forced and subharmonic oscillations in an externally driven single loop relay feedback system (RFS). In the subsequent Chapter 3, the idea of forced oscillations is extended to design dithers in relay feedback systems that will result in stable oscillations of arbitrarily low amplitudes. Chapter 4 examines the conditions for limit cycles in a quantized feedback system under high quantization resolution. Finally, conclusions and suggestions for further works are drawn in Chapter 5.

Chapter 2

Forced and Subharmonic Oscillations under Relay Feedback

2.1 Introduction

In this chapter, the minimum conditions required for FO and SO to occur in a RFS are presented. As a result of the analysis, a fundamental difference between FO and SO was uncovered. In particular, we show that FO is always possible at any frequency if and only if certain minimum conditions on the external signal are met. This, however, does not apply to SO. SO requires specific conditions involving the frequency and amplitude of the external signal. Further new results involving the orders of SO were also obtained from our analysis.

The chapter is organised as follows. The problem formulation is presented in Section 2.2 and the necessary and sufficient conditions for periodic switching and their analysis are shown in Section 2.3. Section 2.4 analyses the existence of the

SO orders, ν, and presents the simulation results. Conclusions are given in Section 2.5.

2.2 Problem Formulation

Consider the RFS with an external forcing signal, $f(t)$, as shown in Figure 2.1. $G(s)$ is a linear system whose state-space representation is

$$\begin{aligned} \dot{z}(t) &= Az(t) + Bu(t-L), \\ c(t) &= Cz(t), \end{aligned} \tag{2.1}$$

where $A \in \mathbb{R}^{m\times m}$ is assumed to be Hurwitz and non-singular; $B \in \mathbb{R}^{m\times 1}$ and $C \in \mathbb{R}^{1\times m}$; $z \in \mathbb{R}^{m\times 1}$ is the state vector; $L \geq 0$ is the time delay; $u(t), c(t) \in \mathbb{R}$ are the input and output, respectively. The ideal relay is given by

$$u(t) = \begin{cases} h, & y(t) < 0; \\ -h, & y(t) \geq 0, \end{cases} \tag{2.2}$$

where $h > 0$ and $y(t)$ is the output of the RFS. The external forcing signal is a sinusoid given by

$$f(t) = R\sin(\omega t + \theta), \tag{2.3}$$

with period denoted by $T = 2\pi/\omega$. Thus,

$$y(t) = c(t) + f(t). \tag{2.4}$$

The transfer function of $G(s)$ is then given by

$$G(s) = \mathrm{e}^{-sL}C(sI - A)^{-1}B.$$

For the simplicity and convenience of our derivation, we assume that the plant is stable, i.e. $\lim_{s\to\infty} G(s) = 0$, and denote the system presented by (2.1)–(2.4) as Σ_L.

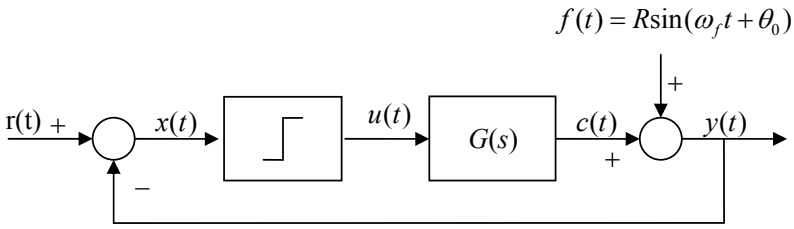

Fig. 2.1. Single loop with external forcing signal.

Define the switching plane

$$\mathcal{F}(t) := \{z(t) : Cz(t) + f(t) = 0\},$$

which is the $(m-1)$-dimension hyperplane where the total output vanishes, as illustrated in Figure 2.2. On either side of $\mathcal{F}(t)$, the feedback system is linear. From (2.1), when $Cz(t)+f(t) > 0$, $\dot{z}(t) = Az(t)-Bh$, while when $Cz(t)+f(t) < 0$, $\dot{z}(t) = Az(t) + Bh$. Since $f(t)$ is an independent input, a sufficiently large $f(t)$ guarantees the consecutive switchings of $z(t)$ on $\mathcal{F}(t)$, which does not tend to any fixed point of the linear system.

Definition 2.1 (Forced and Subharmonic Oscillations)**.** For Σ_L, if there exists $t_f > 0$ and some $t_0 \geq 0$ such that the output of the relay, $u(t)$, satisfies

1. $u(t + t_f/2) \equiv -u(t), \forall t \geq t_0$;

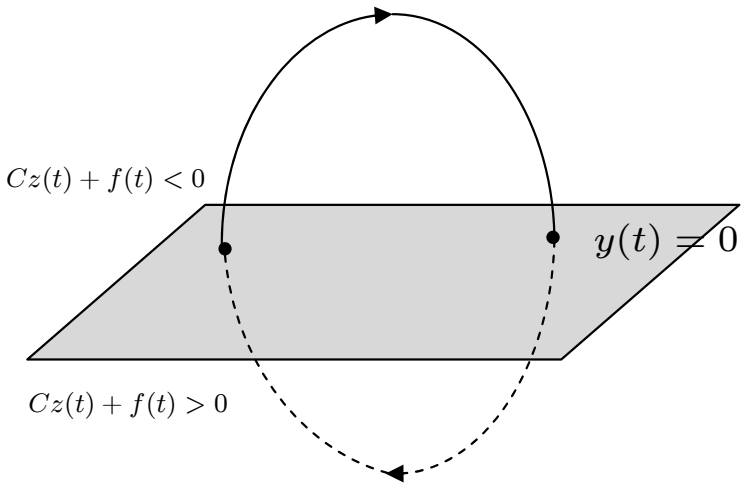

Fig. 2.2. Illustration of switching plane.

2. $T_f = \min\{t_f\} = \nu T = 2\nu\pi/\omega$, $\nu \in \mathbb{N}^+$ is odd,

then $u(t)$ switches periodically with a fundamental period, $T_f = \nu T$, after $t > t_0$. We define *forced oscillation* (FO) to be the case when $\nu = 1$ and *subharmonic oscillation* (SO) corresponds to when $\nu > 1$.

Remark 2.1. The time $t = t_0$ marks either the beginning of or any time after steady state switching has occurred or after all initial transients have decayed. In this chapter, we also assume t_0 to correspond to a positive relay switch.

Remark 2.2. Steady state switching in a RFS is not limited to only FO or SO. There are other types of switchings which are characterised by more complex switchings which are not investigated in this chapter.

Figure 2.3 shows some possible oscillation patterns of Σ_L. The SO in Figure 2.3 is of order $\nu = 3$ because the frequency of $f(t)$ is 3 times that of the relay

switchings. When neither FO or SO exists, self oscillations of frequency ω_s may be seen or some complex switchings may also occur. In Figure 2.3, an example of complex oscillation is shown where the time intervals between relay switchings is not a constant. Sometimes these are referred to as quasi-periodic oscillations.

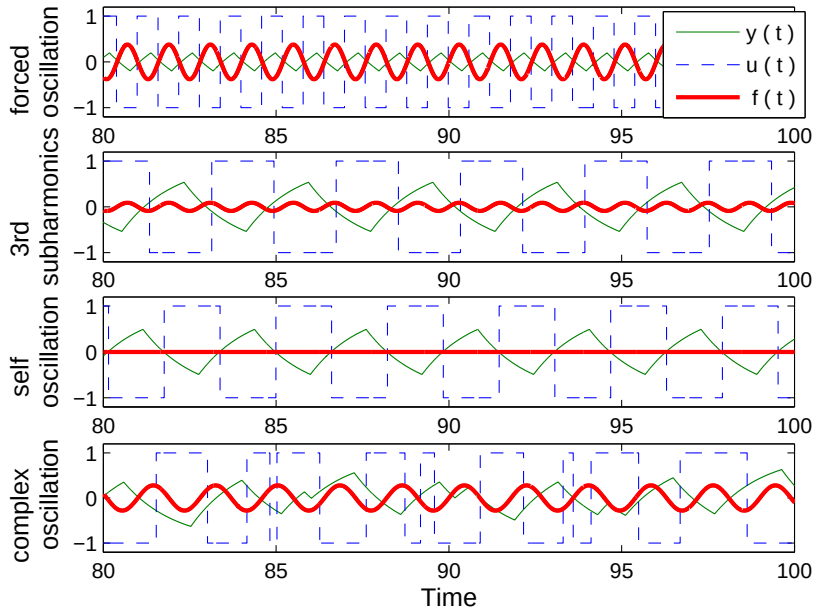

Fig. 2.3. Different oscillations in an externally driven RFS.

For $t > t_0 + \Delta t,\ \Delta t > 0$, following the periodic switchings of the relay, the output, $c(t)$, can be expressed in terms of the frequency responses of the plant

$$c(t_0 + \Delta t) = \frac{4h}{\pi} \sum_{k=\text{odd}}^{\infty} \frac{1}{k} \text{Im} \left\{ G(jk\omega_f) \mathrm{e}^{jk\omega_f \Delta t} \right\}. \tag{2.5}$$

where $\omega_f = 2\pi/T_f$ is the frequency of the relay switchings.

In time domain, by assumption in Remark 2.1, we have the following state

responses :

$$\begin{aligned} \dot{z}(t) &= Az(t) - Bh \quad t \in (t_0, t_0 + L) \\ \dot{z}(t) &= Az(t) + Bh \quad t \in (t_0 + L, t_0 + T_f/2) \end{aligned} \tag{2.6}$$

By solving for $z(t)$ under the constraint that $z(t_0) = -z(t_0 + T_f/2)$, we obtain

$$z(t_0 + \Delta t) = \begin{cases} \mathrm{e}^{At} z(t_0) + \left(I - \mathrm{e}^{A\Delta t}\right) A^{-1} Bh, & \Delta t \in [0, L]; \\ \mathrm{e}^{At} z(t_0) + \left(2\mathrm{e}^{A(\Delta t - L)} - \mathrm{e}^{A\Delta t} - I\right) A^{-1} Bh, & \Delta t \in [L, T_f/2]. \end{cases} \tag{2.7}$$

where $z(t_0) = -\left(I + \mathrm{e}^{AT_f/2}\right)^{-1} \left(2\mathrm{e}^{A(T_f/2 - L)} - \mathrm{e}^{AT_f/2} - I\right) A^{-1} Bh$.

With these in mind, we now investigate: (i) the minimum amplitude R, and, (ii) the frequency ranges (ω) of $f(t)$, for the existence of FO or SO.

2.3 Conditions for Periodic Switching

Without loss of generality, we set $t_0 = 0$ and rewrite Δt as t. At the switching instants corresponding to $t = mT_f/2,\ m = 0, 1, 2, \ldots$, the output, $y(t)$, of Σ_L satisfies

$$y(mT_f/2) = 0,\ (-1)^m \dot{y}(mT_f^-/2) < 0 \tag{2.8}$$

Since (2.8) is imposed only at every half period, it is insufficient to guarantee switchings at only these points, as shown in Figure 2.3. In order to prevent additional switchings in between, another condition is required as follows :

$$(-1)^m y(t) < 0, \quad t \in (mT_f/2, (m+1)T_f/2)\,. \tag{2.9}$$

It is well known that (2.8) is only a necessary condition for switching. It exists only if stability of the limit cycles can be guaranteed. One sufficient condition that

guarantees this stability is given by Atherton (Atherton, 1982) as the following lemma.

Lemma 2.1 (Atherton 1982, (Atherton, 1982)). *For the RFS given by* (2.1)–(2.4)*, stable FO or SO exist if*

$$(-1)^m \dot{y}(mT_f/2) \leq -\frac{2h}{\pi K_c}, \tag{2.10}$$

where K_c is critical gain of the linear element, $G(s)$.

The proof of Lemma 2.1 is based on incremental gain. More details can be found in (Atherton, 1982). With this, we now have the following necessary and sufficient conditions for FO or SO.

Proposition 2.1. *For the RFS in (2.1) - (2.4), FO or SO will exist if and only if the following conditions are satisfied:*

$$\begin{aligned} &\text{(C1)} \quad y(mT_f/2) = 0,\ m = 0, 1, 2, \ldots \\ &\text{(C2)} \quad (-1)^m \dot{y}(mT_f/2) \leq -\tfrac{2h}{\pi K_c} < 0 \\ &\text{(C3)} \quad (-1)^m y(t) < 0 \quad t \in (mT_f/2, (m+1)T_f/2). \end{aligned} \tag{2.11}$$

Proof. Necessity : It is obvious that when stable FO or SO takes place, (C1)-(C3) are satisfied.

Sufficiency : Conditions (C1) and (C2) ensures stable periodic switching at every $t = mT_f/2,\ m = 0, 1, 2, \ldots$ and by further requiring (C3), additional switchings between $t = mT_f/2$ and $t = (m+1)T_f/2$ will not occur. Subsequently, steady periodic switchings are sustained. □

Remark 2.3. The key point is that (C1) and (C3) are only necessary conditions and cannot guarantee stable limit cycles. (C2), on the other hand, guarantees stability and hence the existence of (C1) and (C2).

Remark 2.4. As the conditions in Proposition 2.1 are necessary and sufficient, it suffices to consider (C1) - (C3) for only one half period. Thus in the subsequent analysis, it is convenient to consider only $m = 0$.

As shown in (2.4), the output of the RFS $y(t)$ is a summation of the plant output and the external forcing signal. Thus, the (C1) - (C3) are conditions on the external forcing signal for FO or SO. Proposition 2.1 can now be used to determine the minimum amplitude, R_{min}, of the external sinusoid, $f(t)$, required for FO or SO to occur in the RFS. $R_{\min}$ is determined by

$$R_{\min} = \max\{R_{\min 1}, R_{\min 2}\} \tag{2.12}$$

where $R_{\min 1}$ and $R_{\min 2}$ are the minimum amplitudes of $f(t)$ which satisfy (C1) - (C2), and (C3) respectively.

2.3.1 Determination of $R_{\min 1}$ and $R_{\min 2}$

For the RFS (2.1)–(2.4) under periodic switching with frequency, ω_f, recall from (2.5) (with $t_0 = 0$ and $\Delta t = t$) that

$$c(t) = \frac{4h}{\pi} \sum_{k=\text{odd}}^{\infty} \frac{1}{k} \text{Im}\left\{G(jk\omega_f)\text{e}^{jk\omega_f t}\right\} \tag{2.13}$$

$$\dot{c}(t) = \frac{4h\omega_f}{\pi} \sum_{k=\text{odd}}^{\infty} \text{Re}\left\{G(jk\omega_f)\text{e}^{jk\omega_f t}\right\}. \tag{2.14}$$

Hence, at $t = 0$ (corresponding to $\Delta t = 0$),

$$c(0) = \frac{4h}{\pi} \sum_{k=\text{odd}}^{\infty} \frac{1}{k} \text{Im}\{G(jk\omega_f)\}, \tag{2.15}$$

$$\dot{c}(0) = \frac{4h\omega_f}{\pi} \sum_{k=\text{odd}}^{\infty} \text{Re}\{G(jk\omega_f)\} + h \lim_{s\to\infty} sG(jk\omega_f) \tag{2.16}$$

where $h \lim_{s\to\infty} sG(jk\omega_f)$ represents the steady state gain of the plant. Based on $c(t)$ and $\dot{c}(t)$, the Tsypkin locus ((Tsypkin, 1984; Atherton, 1982)), $\Lambda(\omega_f)$, which is essentially the phase portrait of $c(t)$ at $t = 0$ for different values of ω_f, can be written as :

$$\begin{aligned} \Lambda(\omega_f) &\triangleq \frac{1}{\omega_f}\dot{c}(0) + jc(0) \\ &= \frac{4h}{\pi} \sum_{k=\text{odd}}^{\infty} \left\{ \text{Re}\{G(jk\omega_f)\} + j\frac{1}{k}\text{Im}\{G(jk\omega_f)\} + h \lim_{s\to\infty} sG(jk\omega_f) \right\}. \end{aligned} \tag{2.17}$$

Rewriting $f(t) = R\sin(\omega t + \theta) = R\sin(\nu\omega_f t + \theta)$ the same way and denoting it by $g(\nu, \theta)$, yields

$$g(\nu, \theta) = \frac{1}{\omega_f}\dot{f}(0) + jf(0) = \nu R\cos\theta + jR\sin\theta. \tag{2.18}$$

Since $y(t) = c(t) + f(t)$,

$$\frac{1}{\omega_f}\dot{y}(0) + jy(0) = \Lambda(\omega_f) + g(\nu, \theta).$$

Conditions (C1) and (C2) are thus equivalent to

$$\text{Im}\{\Lambda(\omega_f) + g(\nu, \theta)\} = 0, \tag{2.19}$$

$$\text{Re}\{\Lambda(\omega_f) + g(\nu, \theta)\} < -\frac{2h}{\pi K_c}. \tag{2.20}$$

respectively. If one plots the Tsypkin locus, $\Lambda(\omega_f)$ for arbitrary frequencies of $\omega = \nu\omega_f$ on the complex plane, one may view the vertical line through the point

$(-\frac{2h}{\pi K_c} + j0)$ as the stability line. This line, together with the real axis, divides the complex plane into 4 quadrants and this has substantial significance in the graphical determination of the minimum R required for FO or SO at any frequency. The derivation of this minimum R depends on where the frequency of $f(t)$ lies with respect to these 4 quadrants, and this will be shown later.

Derivation of R_{min1} from conditions (C1) and (C2). It follows from (C1) that

$$\mathrm{Im}\{\Lambda(\omega_f)\} = c(0) = Cz(0) = -\mathrm{Im}\{g(\nu,\theta)\} = -R\sin\theta. \tag{2.21}$$

which yields

$$\theta = \pi + \mathrm{sgn}(Cz(0))\sin^{-1}\left(\frac{|Cz(0)|}{R}\right) = \pi + \mathrm{sgn}(Cz(0))\sin^{-1}\left(\frac{1}{\lambda}\right), \tag{2.22}$$

which requires $\lambda = R/|Cz(0)| \geq 1$. It therefore follows that for any ω,

$$R \geq |Cz(0)|. \tag{2.23}$$

Condition (C2) implies that

$$\mathrm{Re}\{\Lambda(\omega_f) + g(\nu,\theta)\} = \mathrm{Re}\{\Lambda(\omega_f)\} + R\cos\theta \leq -\frac{2h}{\pi K_c}. \tag{2.24}$$

Substituting (2.22) into (2.24) gives

$$\mathrm{Re}\{\Lambda(\omega_f)\} + R\cos\theta = \mathrm{Re}\{\Lambda(\omega_f)\} - \sqrt{R^2 - |Cz(0)|^2} \leq -\frac{2h}{\pi K_c}, \tag{2.25}$$

which is equivalent to

$$\sqrt{R^2 - |Cz(0)|^2} \geq \left(\mathrm{Re}\{\Lambda(\omega_f)\} + \frac{2h}{\pi K_c}\right). \tag{2.26}$$

Two cases of different frequencies are considered.

Case 1 : Frequencies for which $\mathrm{Re}\{\Lambda(\omega_f)\} \leq -2h/(\pi K_c)$ or for which the Tsypkin locus lies to the left of the stability line . In this case, $\mathrm{Re}\{\Lambda(\omega_f)\} + 2h/(\pi K_c) \leq 0$. Since (2.23) is always necessary, therefore (2.26) will never be violated and it follows that minimum R is $|Cz(0)| = |c(0)|$.

Case 2 : Frequencies for which $\mathrm{Re}\{\Lambda(\omega_f)\} > -2h/(\pi K_c)$ or for which the Tsypkin locus lies to the right of the stability line. In this case, $\mathrm{Re}\{\Lambda(\omega_f)\} + 2h/(\pi K_c) > 0$. Solving (2.26) yields

$$R \geq \sqrt{|Cz(0)|^2 + \left(\mathrm{Re}\{\Lambda(\omega_f)\} + \frac{2h}{\pi K_c}\right)^2} = \left|\Lambda(\omega_f) + \frac{2h}{\pi K_c}\right|. \tag{2.27}$$

Hence the minimum R is at least $\left|\Lambda(\omega_f) + \frac{2h}{\pi K_c}\right|$.

In summary, from (C1) and (C2), we have the following conditions for R_{min1} :

$$R_{\min 1} = \begin{cases} |\mathrm{Im}\{\Lambda(\omega_f)\}| = |c(0)|, & \text{if } \mathrm{Re}\{\Lambda(\omega_f)\} \leq \mathrm{d}\frac{-2h}{\pi K_c} \quad (2.28a) \\ \left|\Lambda(\omega_f) + \mathrm{d}\dfrac{2h}{\pi K_c}\right|, & \text{if } \mathrm{Re}\{\Lambda(\omega_f)\} > \mathrm{d}\frac{-2h}{\pi K_c} \quad (2.28b) \end{cases}$$

R_{min1} can always be obtained graphically from a plot of $\Lambda(\omega_f)$.

On the complex plane, consider quadrants which are numbered anticlockwise from 1 to 4 starting from the top right hand region to the right of the stability line. An example of this is illustrated in Figure 2.4. For ω_f in each of these quadrants, the following holds :

$$\text{Quadrants 1 \& 4 :} \quad \mathrm{Re}\{\Lambda(\omega_f)\} > \mathrm{d}\tfrac{-2h}{\pi K_c}, \quad \lambda > 1$$

$$\text{Quadrants 2 \& 3 :} \quad \mathrm{Re}\{\Lambda(\omega_f)\} \leq \mathrm{d}\tfrac{-2h}{\pi K_c}, \quad \lambda = 1$$

As θ depends on the sign of $Cz(0)$, its value can also be visualized graphically. In quadrants 1 and 4 where $\lambda > 1$, θ is computed according to (2.22). In quadrants 2 and 3 where $\lambda = 1$, $\theta = 0.5\pi$ and $\theta = 1.5\pi$ respectively. A summary of R_{min1}

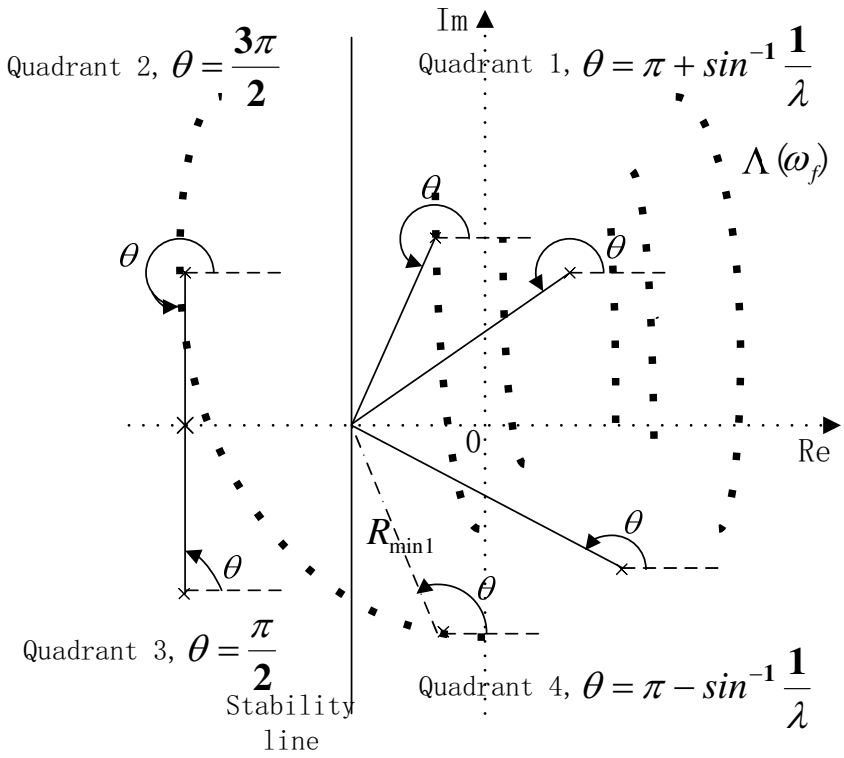

Fig. 2.4. Illustration of θ on the complex plane.

and θ is as follows :

$$\text{Quadrants 1 \& 4:} \quad R_{\min 1} = \left|\Lambda(\omega_f) + \frac{2h}{\pi K_c}\right| = \lambda |Cz(0)|,$$
$$\theta = \pi + \operatorname{sgn}(Cz(0)) \sin^{-1}\left(\frac{1}{\lambda}\right)$$
$$\text{Quadrants 2 \& 3:} \quad R_{\min 1} = |\operatorname{Im}\{\Lambda(\omega_f)\}| = |Cz(0)|,$$
$$\theta = \frac{3\pi}{2} \text{ or } \frac{\pi}{2}.$$

Remark 2.5. It should be noted that θ corresponds to the phase at absolute $t = t_0$, as opposed to the original θ of $f(t)$. This notation is consistent when t_0 is assumed to be zero.

Derivation of R_{min2} from conditions (C3). Condition (C3) requires

$$y(t) < 0, \quad t \in (0, T_f/2)\,, \tag{2.29}$$

which, by (2.3) and (2.4),

$$y(t) = c(t) + f(t) = c(t) + R\sin(\omega t + \theta). \tag{2.30}$$

Substituting (2.22) and (2.30) into (2.29) yields,

$$\begin{aligned} y(t) &= c(t) + R\sin(\omega t)\cos\theta + R\cos(\omega t)\sin\theta \\ &= c(t) - \sin(\omega t)\sqrt{R^2 - (Cz(0))^2} - \cos(\omega t)Cz(0) < 0, \end{aligned}$$

which leads to

$$\sqrt{R^2 - (Cz(0))^2} > \frac{c(t) - Cz(0)\cos(\omega t)}{\sin(\omega t)}, \quad t \in (0, T_f/2). \tag{2.31}$$

Since $\omega = \nu\omega_f$, the right hand side of (2.31) is always finite for $\nu = 1$. Hence, one can always find an R_{min2} as follows :

$$R_{min2} = \max_{t\in(0,T_f/2)} \frac{c(t) - Cz(0)\cos(\omega t)}{\sin(\omega t)}. \tag{2.32}$$

Since (C1) - (C3) are necessary and sufficient conditions for steady state oscillations, the overall minimum R should be

$$R_{\min} = \max\left\{R_{\min 1}, R_{\min 2}\right\}. \tag{2.33}$$

R_{min1} relates to the minimum amplitude of $f(t)$ required to achieve periodic switching at intervals of $T_f/2$, whereas R_{min2} relates to the minimum amplitude of $f(t)$ required for no additional switchings in between periods. Therefore, for any $f(t)$ with frequency ω, FO at frequency $\omega_f = \omega$ is always possible as long as its amplitude, R, is set to be at least larger than R_{min}.

For SO corresponding to $\nu > 1$, the RHS of (2.31) may become positively infinite for some values of $t = mT_f/(2\nu)$ where $m < \nu$. When this happens, a finite

solution to (2.31) may not exists and SO fails. However, there are some frequencies, ω, where the response, $c(t)$ at $t = mT_f/(2\nu)$, is such that the numerator of (2.31) is negative when the denominator is zero. For such cases, the RHS of (2.31) is negative infinity at these time instants and any $R \geq |Cz(0)|$ satisfies (2.31) at that time instant. When this occurs, R_{min2} is once again given by (2.32) and SO becomes possible for these frequencies.

The following example demonstrates this problem.

Example 2.1. Consider a second order system with

$$A = \begin{bmatrix} 0 & 1 \\ -4 & -6 \end{bmatrix}, \; B = \begin{bmatrix} 0 \\ 4 \end{bmatrix}, \; C = \begin{bmatrix} 1 & 0 \end{bmatrix}, \; L = 1. \tag{2.34}$$

For this plant, the stability line corresponds to a vertical line at $\mathrm{d} - \frac{2h}{\pi K_c} = -0.248$. Figure 2.5 plots the Tsypkin locus for a range of frequencies, $n\pi/L < \omega_f \leq (n+1)\pi/L, \; n = 0, 1, 2$. Note that the range of frequencies is deliberately parameterized in terms of integer values of n and the delay term, L. The significance of this will be obvious in Section 2.4. Consider the frequency of 0.6 rad/s on $\Lambda(\omega_f)$ which is to the right of the stability line or in Quadrant 4, R_{min1} is as indicated in Figure 2.5. Figure 2.6 shows the plot of R_{min1}, R_{min2} from calculations, and R_{min} from simulation. It can be observed that for $\omega_f \geq 0.8$, $R_{min} = R_{min1} \approx R_{min2}$. For $\omega_f < 0.8$, R_{min} is determined by R_{min2}. For higher frequencies corresponding to $n = 1$ and $n = 2$, R_{min} is better predicted by R_{min1}. The predicted $R_{min} = \max(R_{min1}, R_{min2})$ are close to the simulated values. It is thus verified that $\max(R_{min1}, R_{min2})$ can indeed provide the R_{min} required. For this plant, it

can be checked that SO does not exist at every frequency. For example, at $\omega_f = 3$ rad/s, no SO can be obtained no matter how large R is.

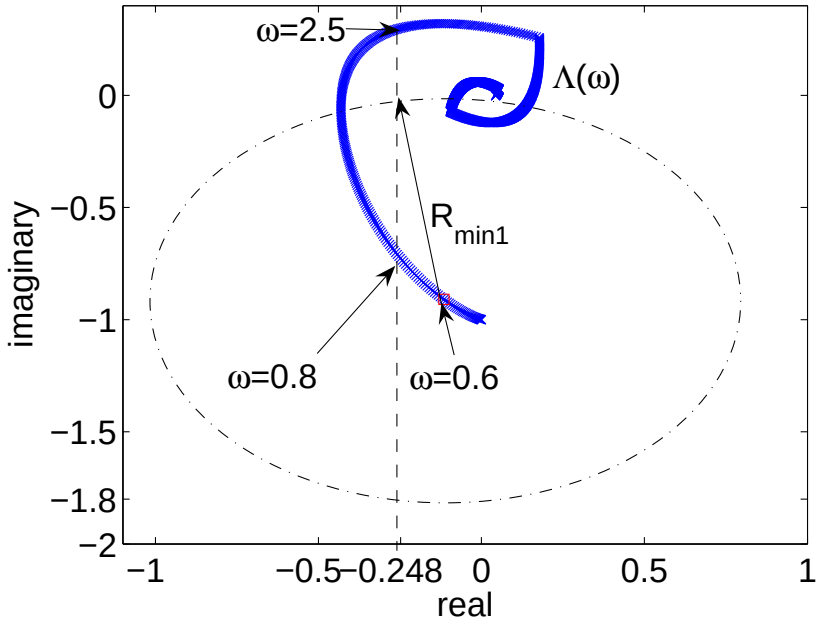

Fig. 2.5. Tsypkin locus for a second order plant.

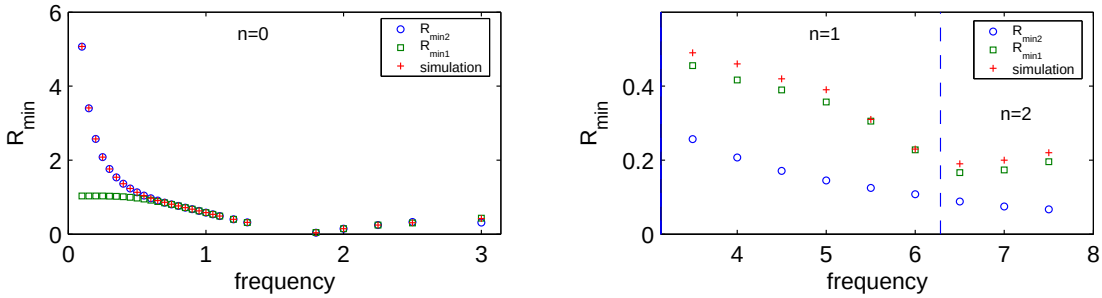

Fig. 2.6. R_{min} comparison for plant in (2.34).

2.3.2 Frequency Ranges of External Signal for SO

Section 2.3.1 shows how SO may not always be possible depending on the inequality of (2.31) which, in turn, depends on the specific frequency of $f(t)$. It was shown

that the existence of SO requires the following condition :

$$c(t) - Cz(0)\cos\omega t < 0 \text{ at } t = mT_f/(2\nu),\ m < \nu. \tag{2.35}$$

By analysing (2.35) carefully, the range of ω for the existence of SO can be determined. The result is captured in the following proposition.

Proposition 2.2. *SO is possible for all frequencies, $\omega \in \Omega$, where*

$$\Omega = \bigcap \Omega_m, \quad m = 1, 2, \cdots, \nu - 1, \tag{2.36}$$

and Ω_m is the solution set of ω for the following inequalities:

$$Ce^{A\frac{m\pi}{\omega}} z(0) + C\left(I - e^{A\frac{m\pi}{\omega}}\right) A^{-1}Bh + (-1)^{m+1}Cz(0) < 0, \qquad t \in (0, L), \tag{2.37}$$

$$Ce^{A\frac{m\pi}{\omega}} z(0) + C\left(2e^{A\left(\frac{m\pi}{\omega} - L\right)} - e^{A\frac{m\pi}{\omega}} - I\right) A^{-1}Bh + (-1)^{m+1}Cz(0) < 0, \qquad t \in (L, \nu T/2). \tag{2.38}$$

Furthermore, the minimum R required of $f(t)$ satisfies (2.33).

Proof. It was established in Section 2.3.1 that the frequencies for which SO is possible satisfy (2.35). Accordingly, at $t = mT_f/(2\nu) = mT/2$, (2.35) becomes

$$c(mT/2) - Cz(0)\cos m\pi < 0, \quad m = 1, 2, \ldots, \nu - 1 \tag{2.39}$$

Using $c(t) = Cz(t)$ with $z(t)$ from (2.7), we have

$$c(mT/2) = \begin{cases} C\left[e^{mAT/2}z(0) + \left(I - e^{mAT/2}\right) A^{-1}Bh\right], & t \in [0, L]; \\ C\left[e^{mAT/2}z(0) + \left(2e^{A(mT/2 - L)} - e^{mAT/2} - I\right) A^{-1}Bh\right], & t \in [L, \nu T/2] \end{cases} \tag{2.40}$$

where

$$z(0) = -\left(I + e^{AT_f/2}\right)^{-1} \left(2e^{A(T_f/2 - L)} - e^{AT_f/2} - I\right) A^{-1}Bh.$$

Since $\cos m\pi = (-1)^m$, (2.39) leads to (2.37) and (2.38) using (2.40). For each m, inequalities (2.37) and (2.38) admit possible ranges of frequencies, Ω_m. The total solution is therefore an intersection of all possible intervals ie $\Omega = \bigcap \Omega_m,\ m = 1, 2, \ldots, \nu - 1$. Finally, the requirement of R_{min} follows from Section 2.3.1. □

In summary, therefore, if one wishes to determine if SO of order ν is possible using an external signal, $f(t) = \sin(\omega t + \theta)$, then T which corresponds to ω should first satisfy (2.37) and (2.38). Subsequently, the minimum $R_{\min}$ which enforces this SO can be derived from $R_{\min} = \max\{R_{\min 1}, R_{\min 2}\}$. Similarly, if one wishes to enforce FO in the RFS, then one should set R according to the same R_{min} formula. No frequency check is required since FO is always possible as long as $R > R_{min}$.

It should be clear at this stage that R_{min} has a complex relationship with the frequency, ω, in the case of FO. In the case of SO, this relationship is further complicated by the order, ν, at which SO can exists. Specifically, given ω, several orders of SO may be possible and thus for each, ν, there is an associated R_{min}. Let this ν-specific R_{min} be denoted by $R_{\nu,min}$. Its dependency on frequency is ignored in order not to complicate the notation.

Suppose $\Omega = [\omega_1, \omega_2]$. Then the above analysis implies that for a given $f(t)$ with an amplitude R and frequency ω, if

$$R_{1,min} > R \geq R_{\nu,min}, \quad \nu > 1, \tag{2.41}$$

then since $R < R_{1,min}$, FO cannot happen but SO of order ν should be observable in the RFS. This is demonstrated in the following example.

Example 2.2. Consider a FOPDT plant

$$G(s) = \frac{1}{s+1}\mathrm{e}^{-s}$$

with $A = B = C = L = 1$ and zero initial conditions. Values of $R_{\nu,min}$ are plotted against $T/2$ in Figure 2.7 where $\omega = 2\pi/T$ is the frequency of $f(t)$. If $T/2$ falls within the bounds indicated in Figure 2.7 for each ν and $R_{1,\min} > R \geq R_{\nu,\min}$, we expect that SO of order ν will be observed. For example, for $\nu = 3$, SO will occur for the range $0.418 < T/2 < 0.643$ obtained from (2.37) and (2.38). If $f(t)$ has $T/2 = 0.6$, then $R_{1,\min} = 0.545$ and $R_{3,\min} = 0.2288$. If $R = 0.2289$ is set, then SO of order 3 occurs with this $f(t)$. This is illustrated in Figure 2.8 where the frequency of $f(t)$ is 3 times that of the relay switches. Note that although the self oscillating period $T_s = 3.019s$, the third subharmonic is achieved for $2.508 < 3T < 3.8580$. The 3rd subharmonic exists with a period around that of self oscillation.

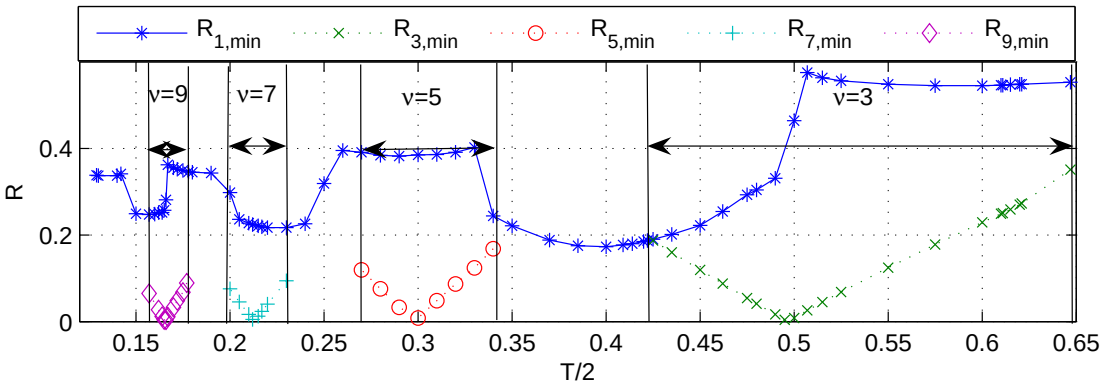

Fig. 2.7. Dependence of SO on R and $T/2$.

Observe also that for a particular R in Figure 2.7, SO of different νs should theoretically be possible by varying the frequency of $f(t)$. Figure 2.9 shows a plot

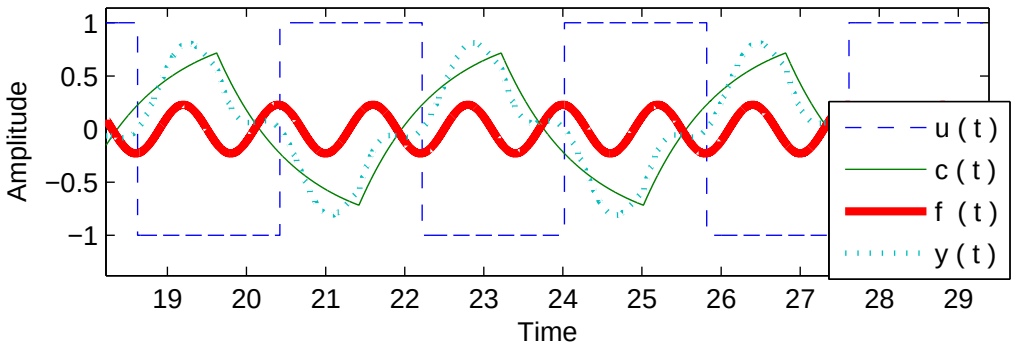

Fig. 2.8. Example where the desired SO with $\nu = 3$ is obtained.

of the relay switching intervals against t_i for a constant $R = 0.145$ where t_i denotes the integer number of relay switches. The frequency of $f(t)$ was varied by varying $T/2$ in the simulation to obtain the different orders of SO. As can be seen, in the first set of 60 switches, $f(t)$ has a frequency corresponding to $T/2 = 0.16$ and the figure indicates that the relays were switching at intervals of $(9 \times 0.16 = 1.44)$ which means SO of $\nu = 9$ is taking place. In the next set of switches from $t_i = 60$ to $t_i = 110$, $T/2$ was changed to 0.165 and this resulted in relay switching intervals of $(0.165 \times 9 = 1.485)$ which still implies SO of order 9. Subsequently, after more changes in $T/2$, at about $t_i = 250$, with the same R but $T/2 = 0.2$, the relay switching interval drops to $(0.2 \times 7 = 1.4)$ which implies SO of order 7. This interesting set of results illustrates the complex relationship between T, ν and R.

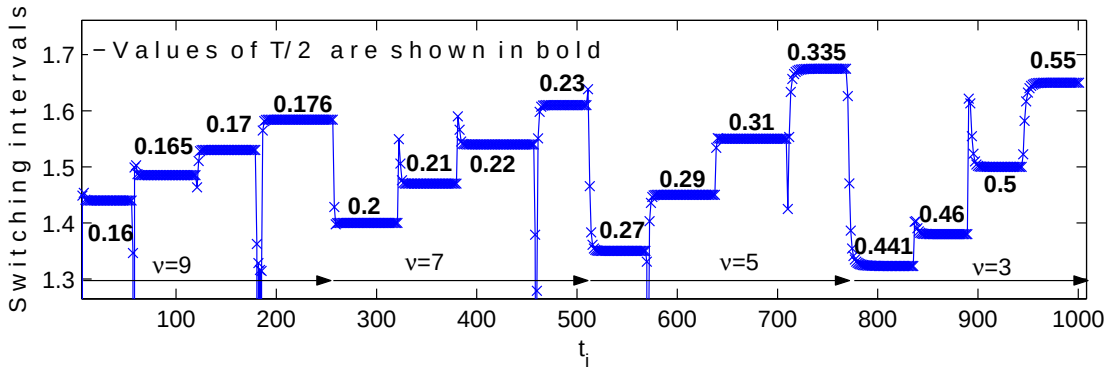

Fig. 2.9. Different νs obtained with a fixed R and varying $T/2$.

2.4 Limits of ν in SO

The results thus far have focused on the requirement of R and ω in $f(t)$ which will cause FO or SO in a RFS. In the case of SO, further analysis is necessary to determine whether there are fundamental limits imposed by the structure of $G(s)$ on the limits of ν in the SO. The question is whether any order is always possible or are there upper limits of ν for a given plant? This problem is addressed in this section.

2.4.1 SO analysis for first order plants

Corollary 2.1. *For first order plants without delay ($L = 0$) in the RFS of Figure 2.1, it is not possible for SO of any order to exist.*

Proof. According to Proposition 2.2, the left hand side (LHS) of (2.38) satisfies

$$LHS = 2C(I + e^{A\nu\frac{T}{2}})^{-1}[e^{AmT/2} - I]A^{-1}Bh > 0 \quad \text{for all } \nu. \tag{2.42}$$

Since (2.42) violates (2.38) for all ν, no SO can take place for this class of plants. □

Corollary 2.2. *For FOPDT plants,*

1. *SO of order $\nu \geq 2n+3$ cannot exist, where $n \in \mathbb{Z}^+$ is determined by*

$$nT/2 < L < (n+1)T/2. \tag{2.43}$$

2. *For each order $\nu < 2n+3$, the range of T is bounded by*

$$\frac{\Gamma}{(\nu+1)A} < \frac{T}{2} < \frac{\Gamma}{(\nu-1)A}, \tag{2.44}$$

where $\Gamma = \ln(e^{AL} + e^{A(\nu\frac{T}{2}+L)} - e^{A\nu\frac{T}{2}})$. Furthermore, this range of frequencies does not overlap for adjacent orders, ν and $\nu+2$.

Proof. (i) At $t = mT/2$, when m is an even positive integer and $m < \nu$, substituting $L < (n+1)T/2$ into the LHS of (2.38), we have

$$\begin{aligned}
LHS &= 2C(I + e^{A\nu\frac{T}{2}})^{-1}[e^{A(\nu\frac{T}{2}-L)} + e^{A(m\frac{T}{2}-L)} - e^{A(\nu\frac{T}{2})} - I]A^{-1}Bh \\
&> 2C(I + e^{A\nu\frac{T}{2}})^{-1}[e^{A(\nu\frac{T}{2}-(n+1)\frac{T}{2})} + e^{A(m\frac{T}{2}-(n+1)\frac{T}{2})} - e^{A(\nu\frac{T}{2})} - I]A^{-1}Bh \\
&= 2C(I + e^{A\nu\frac{T}{2}})^{-1}[(e^{A}(n+1)\frac{T}{2} - I)(I - e^{A(\nu\frac{T}{2}-(n+1)\frac{T}{2})})]A^{-1}Bh \\
&> 0 \quad \text{for } \nu > 2(n+1)
\end{aligned}$$

Hence the violation of (2.38) occurs for $\nu > 2(n+1)$. Therefore SO of order $\nu \geq 2n+3$ cannot exists.

(ii) Analysis of (2.37) and (2.38) for FOPDT plants leads to

$$\frac{T}{2} > \frac{1}{(\nu+1)A}\Gamma \tag{2.45}$$

$$\frac{T}{2} < \frac{1}{(\nu-1)A}\Gamma, \tag{2.46}$$

respectively, where $\Gamma = \ln(e^{AL} + e^{A(\nu\frac{T}{2}+L)} - e^{A\nu\frac{T}{2}}) > 0$. Thus for each $\nu < 2n+3$, the frequency range for each ν is

$$\frac{\Gamma}{(\nu+1)A} < \frac{T}{2} < \frac{\Gamma}{(\nu-1)A}.$$

Next we show that the range of T for adjacent orders, ν and $\nu+2$ does not overlap. Consider two adjacent ν's, $\nu = 2j-1$ and $\nu = 2j+1$. For each ν, the range of $T/2$ is given by

$$\left.\begin{array}{l} \nu = 2j-1 \\ \\ \\ \\ \nu = 2j+1 \end{array}\right\} \begin{array}{l} \frac{T}{2} > \frac{1}{(2j-1)A}\ln(e^{AL} - e^{A2j\frac{T}{2}}) - \ln(I - e^{AL}) = C_1 \\ \\ \frac{T}{2} < \frac{1}{(2j-1)A}\ln(e^{AL} - e^{A(2j-2)\frac{T}{2}}) - \ln(I - e^{AL}) = C_2 \\ \\ \frac{T}{2} > \frac{1}{(2j+1)A}\ln(e^{AL} - e^{A(2j+2)\frac{T}{2}}) - \ln(I - e^{AL}) = C_3 \\ \\ \frac{T}{2} < \frac{1}{(2j+1)A}\ln(e^{AL} - e^{A2j\frac{T}{2}}) - \ln(I - e^{AL}) = C_4. \end{array}$$

Thus

$$\begin{aligned} \nu = 2j-1 \quad &: \quad C_1 < T/2 < C_2 \\ \nu = 2j+1 \quad &: \quad C_3 < T/2 < C_4 \\ &\qquad C_4 < C_1 \end{aligned}$$

Therefore the range of frequencies for $\nu = 2j-1$ and $\nu = 2j+1$ where $j \in \mathbb{N}^+$, does not overlap. This is illustrated in Figure 2.10. □

Example 2.3. For a FOPDT plant, where $A = -1/3$, $B = 1$, $C = 1/3$ and $L = 2$, the bounds of T for each ν can be calculated from (2.44). These are plotted in Figure 2.10 along with the possible ν's obtained from simulations. Figure 2.10 also indicates the partitioning of T in terms of n according to (2.43). This figure also

confirms that SO of order $\nu \geq 2n+3$ cannot occur for this plant. For example, for $n = 2$, $\nu \geq 7$ cannot be obtained but $\nu = 3, 5$ are both possible. It can also be observed that there are no overlaps in frequency for two adjacent orders.

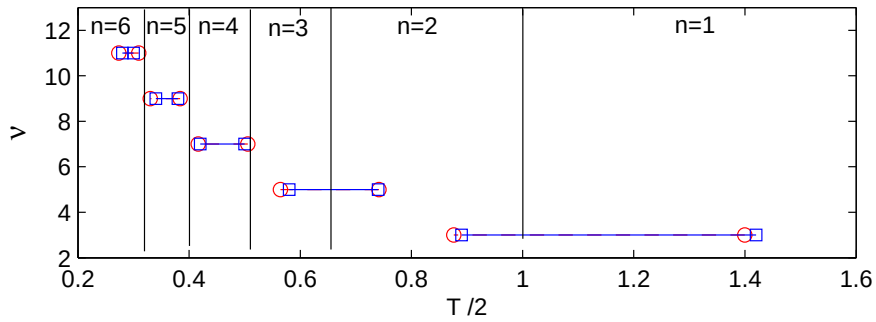

Fig. 2.10. Plot of the bounds for example 2.3, 'o': Calculated, '□':Simulated.

2.4.2 SO analysis for higher order plants

The SO analysis for higher order systems is not as easy as first order plants. Nevertheless, some observation can still be obtained. For example, SO of order $\nu \geq 2n+3$ can exist and the range of T for each ν is not distinct. We show these observations through a few examples.

Example 2.4. Consider a third order delayed plant, $G(s) = \frac{e^{-s}}{(s+1)^3}$. The range of $T/2$ for which each ν exists is plotted in Figure 2.11. It can be observed that for some $T/2$, SO of order $\nu \geq 2n+3$ cannot be excluded. For example, for $n = 1$, SO of orders $\nu = 3, 5, 7$ are possible. However, in this example, the frequency ranges are also distinct.

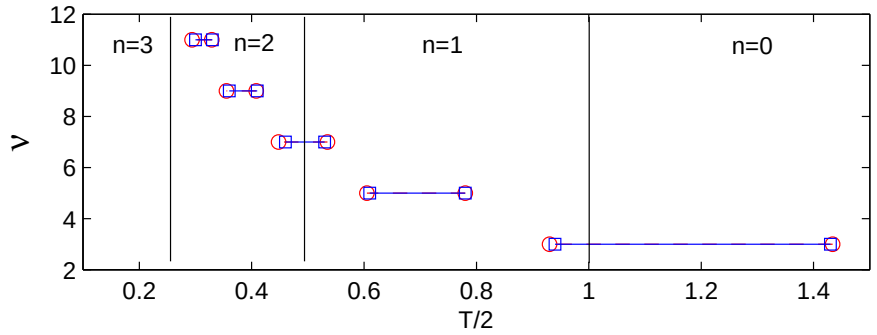

Fig. 2.11. Plot of the bounds for example 2.4, 'o': Calculated, '□':Simulated.

Example 2.5. Consider a fourth order non-delayed plant, $G(s) = \frac{-s+0.2}{s^4+2s^3+1.31s^2+0.34s+0.03}$. In this case, T cannot be parameterized in terms of n. Nevertheless, Figure 2.12 also shows the distinctiveness of the frequency ranges for each ν.

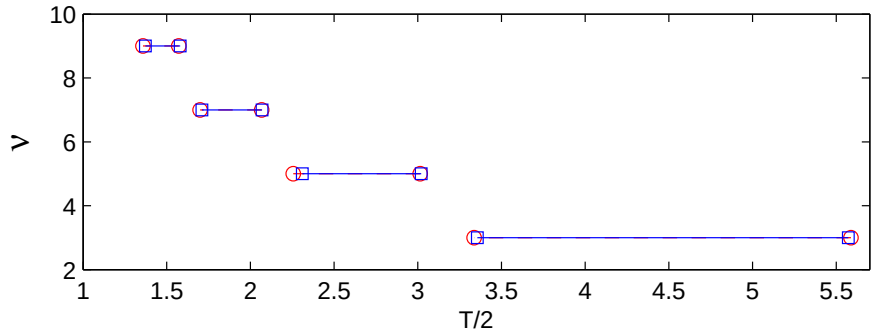

Fig. 2.12. Plot of the bounds for example 2.5, 'o': Calculated, '□':Simulated.

Example 2.6. Consider a second order non-delayed plant, $G(s) = \frac{-s+0.2}{s^2+6s+7}$ with zero initial state vector. Figure 2.13 shows the plot of the calculated bounds and the simulated bounds for $\nu = 3, 5, 7$. These bounds overlap one another, indicating that multiple orders of SO are possible for a single frequency of $f(t)$. The actual ν that occurs depend on the magnitude of R.

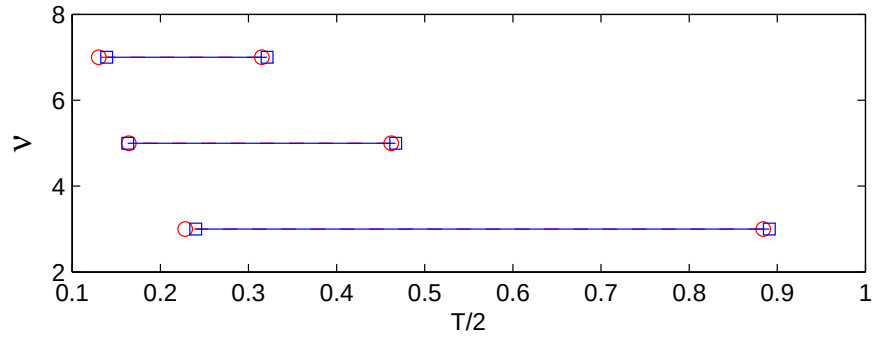

Fig. 2.13. Plot of bounds for example 2.6, 'o': Calculated, '□':Simulated.

Figure 2.14 is a plot of the relay switching time intervals when the RFS was driven by a $f(t)$ with varying amplitude, R, and fixed frequency corresponding to $\frac{T}{2} = 0.12$. The amplitude R was varied according to the values in Table 2.1. Initially, with $R = 0.12$ and FO ($\nu = 1$) was observed. After a period of time, R was changed to $R = 0.0871$ and $\nu = 9$ was observed even though the frequency of $f(t)$ remained unchanged. By changing R further, SO with $\nu = 11, 13, 15, 17$ were observed. This example shows that several νs can occur for a given $T/2$ depending on the magnitude, R, of $f(t)$.

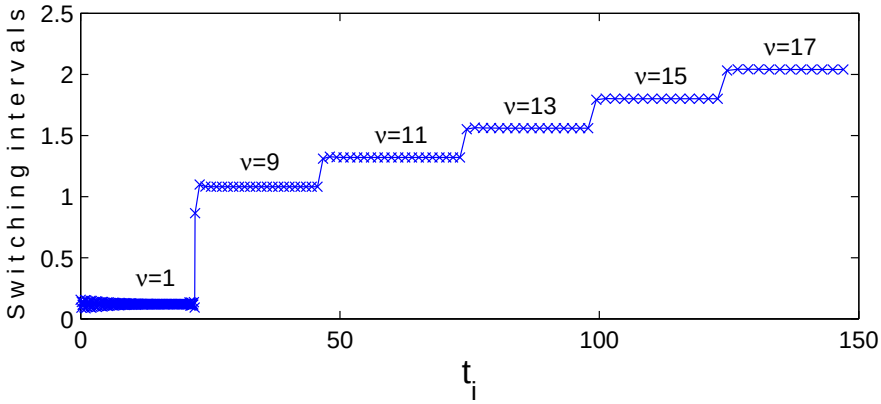

Fig. 2.14. Multiple νs of SO observed for example 2.6 with varying R.

Table 2.1. Table of R and $R_{\nu,min}$ for example 2.6.

ν	1	9	11	13	15	17
$R_{\nu,min}$	0.11	0.087	0.057	0.033	0.015	0.0015
R	0.12	0.0871	0.0571	0.0331	0.0151	0.0016

Example 2.7. In this example, $G(s) = \frac{s+0.2}{s^4+0.03s+0.34s^2+1.31s+2}$ was simulated with zero initial conditions. The bounds of $T/2$ (through the simulation) for each ν are shown in Figure 2.15. It appears that the predicted bounds are not accurate when compared to the simulated bounds.

At $T/2 = 0.699$, when the initial state vector was changed to $z(0) = [-0.3955; -0.4220; 0.09896; 0.1838]$ and $f(t)$ was set with $R = 0.1358 > R_{3,min} = 0.1357$ and $\theta = 4.6783$ rad, SO of order $\nu = 3$ occurred at the first switch. When θ was reset to $\theta = 0$, $\nu = 5$ occurred after some initial transients. The oscillations are shown in Figure 2.16. This result suggests that initial conditions also play a role in determining what is achievable in terms of ν. By further varying initial conditions and θ, it was possible to obtain simulation bounds which are closer to our calculations. This is shown in Figure 2.17 for the same $G(s)$. The calculated and simulated bounds are now almost identical. The effect of varying the initial state vector is best illustrated in Figure 2.18 which is a plot of the state z_3 against z_4. R is fixed at 0.26931 and the initial state vector, z_0 is varied from [0;0;0;0] to [1;1;0;0.5]. It can be seen that the trajectories of $z(t)$ tend towards two different limit cycles of orders, $\nu = 3$ and $\nu = 5$. Interestingly, our analysis appears to give tight bounds of the frequencies even though the complexities due to initial

conditions were never considered in our analysis.

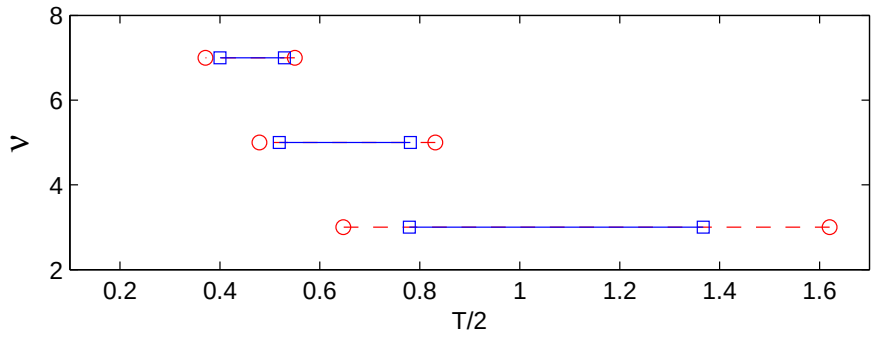

Fig. 2.15. Effect of only varying R for example 2.7, 'o': Calculated bounds, '□':Simulated bounds.

2.5 Conclusion

In this chapter, the conditions for stable FO and SO to occur in a sinusoidally forced single loop RFS were examined. It was found that the external forcing signal requires a minimum amplitude, R_{min}, for either FO or SO to occur. A combination of a graphical approach using the Tsypkin Locus and a numerical approach was used to determine this R_{min}.

The main contribution of this chapter lies in the discovery of the fundamental difference between FO and SO. FO is possible for any frequency of the external forcing signal as long as its amplitude was sufficiently large. This was however not the case for SO. A complex relationship between frequency, amplitude and ν exists for SO. Specifically, not all forcing signals can drive the RFS at any order ν (except $\nu = 1$) even if the amplitude of the external signal is large. The ranges of

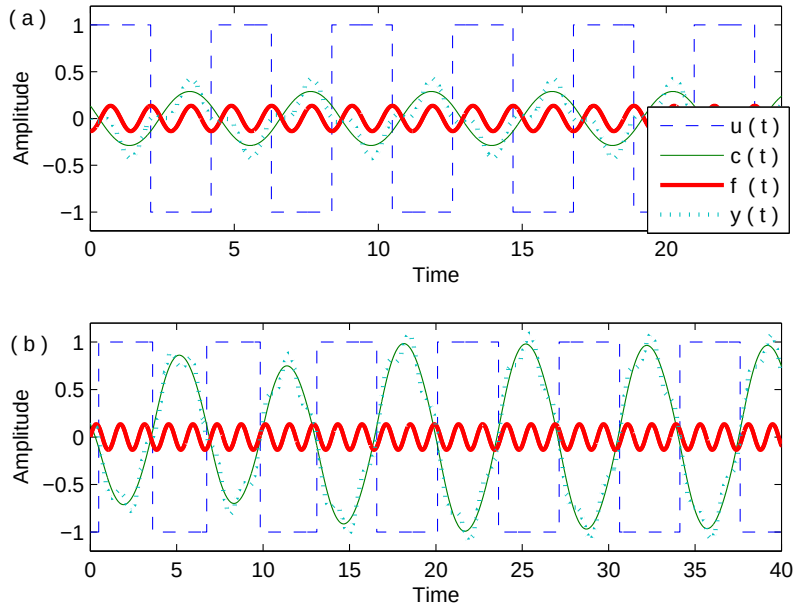

Fig. 2.16. (a) SO of $\nu = 3$ obtained with $\theta = 4.6783$. (b) SO of $\nu = 5$ obtained with $\theta = 0$.

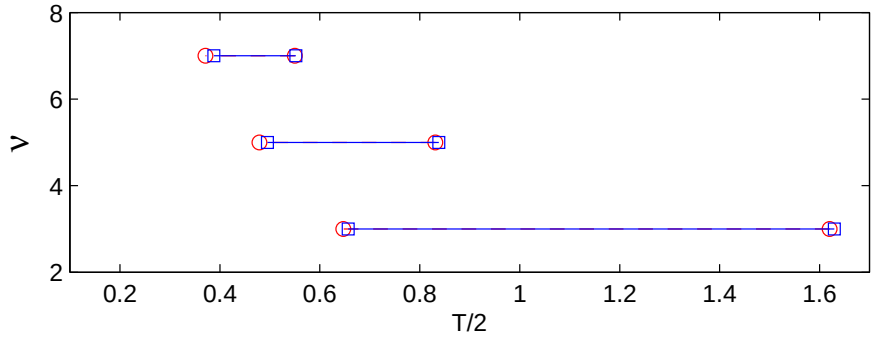

Fig. 2.17. Effect of varying R, z_0 and θ for example 2.7, 'o': Calculated bounds, '□':Simulated bounds.

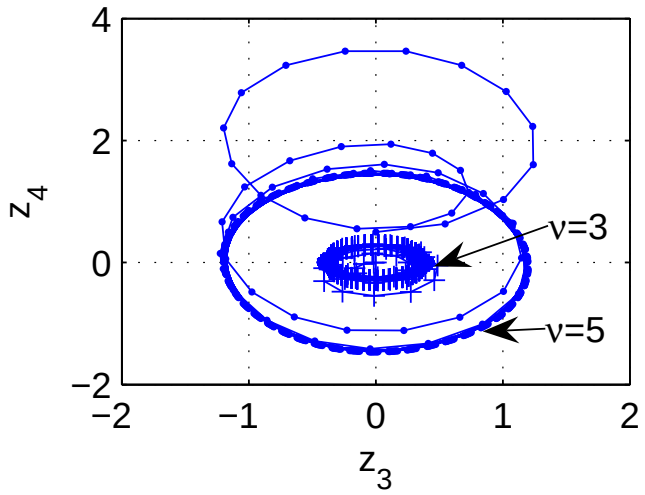

Fig. 2.18. Effect of the initial condition for example 2.7.

frequencies where SO of certain orders can be obtained were derived. Results for FOPDT plants were completely given. Other behaviours for higher order plants were also presented.

Chapter 3

Design of Amplitude Reduction Dithers in Relay Feedback Systems

3.1 Introduction

In our previous chapter on forced oscillation in RFS, we have given very specific conditions for the design of external sinusoidal dither signals that can induce oscillations of the same frequency as this dither signal. The analysis given was exact and does not rely on any approximation theory. The results were also necessary and sufficient. In this chapter, we extend the results in Chapter 2 to design sinusoidal dither signals that will result in stable oscillations of arbitrarily low amplitudes.

The use of dithers to achieve signal stabilization and quenching of limit cycles is well known in nonlinear systems. The idea is similar to the phenomenon of

forced oscillations (FO). This idea is used to design a dither signal which results in reduced oscillation amplitudes. Our analysis applies to any periodic symmetric dither signals of other shapes. This is because as long as the dither amplitude is sufficiently large to induce forced oscillations of period T_f in the system, the input to the plant is always a symmetric square wave due to the relay switchings. Thus the plant's steady state output is only dependent on the relay's switching period T_f and is independent of the actual shape of the dither signal. Therefore, the identification of the bound on the dither period in this chapter can be applied to other dither shapes.

This chapter is organized as follows. The problem formulation is presented in Section 3.2. Section 3.3 presents the numerical approach to identify the bound on the dither period. Complete solutions for first and second order plants will be presented in Section 3.5. Section 3.6 shows that the analysis can be used with other dither shapes. Applications on the missile roll control system and the control of a DC motor are given in Section 3.7. Section 3.8 presents the conclusions.

3.2 Problem Formulation

Consider the RFS with a sinusoidal dither signal, $f(t)$, as shown in Fig. 3.1. The linear system, $G(s)$, is assumed to have a state space description and together with

the relay element, the closed loop RFS is given by

$$\dot{z}(t) = Az(t) + Bu(t-L) \tag{3.1}$$

$$c(t) = Cz(t) \tag{3.2}$$

$$y(t) = c(t) + f(t) = c(t) + R\sin(\omega_f t) \tag{3.3}$$

$$u(t) = \begin{cases} h & y(t) < 0 \\ -h & y(t) \geq 0 \end{cases} \tag{3.4}$$

where $h > 0$, $u, c \in R$ are the plant's input and output, respectively, $z \in R^{m\times 1}$ is the state vector, $L > 0$ is the time delay between u and c, $A \in R^{m\times m}$ is Hurwitz and assumed to be non-singular, $B \in R^{m\times 1}$ and $C \in R^{1\times m}$. In the frequency domain, $G(s) = e^{-sL}C(sI - A)^{-1}B$ and $\lim_{s\to\infty} G(s) = 0$. Under these conditions, the RFS would generally exhibit oscillatory behaviour. The problem we address is

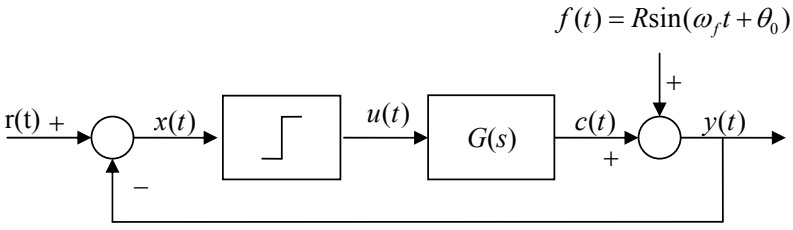

Fig. 3.1. RFS with external forcing signal.

the design of $f(t)$ to achieve a reduction in the amplitude of oscillations in the RFS. The approach is based on the concept of forced oscillations (FO) (Tsypkin, 1984). Our analysis starts with the identification of the bound, T_f^*, below which the oscillation amplitude decreases monotonically as T_f decreases. This analysis is only meaningful if we are able to ensure that FO exists for any T_f. It has been shown in

Chapter 2 that FO exists if and only if $R \geq R_{min}$. Using a high R_{min} will not induce high oscillations in the system as the relay output into the plant is at a fixed height. The switching of the relay under FO induces smaller oscillations, as compared to self oscillations. This method differs from variable structure controllers like sliding mode controllers as only the feedback is the error signal. In order to facilitate the discussion and analysis, the results on the conditions for FO are reproduced from Chapter 2 as follows :

Proposition 3.1. *For the RFS in (3.2)-(3.4), FO exists with frequency ω_f if and only if the amplitude, R, of the sinusoidal dither, $f(t) = R\sin\omega_f t$, satisfies $R \geq R_{min}$ where*

$$R_{min} = \max\{R_{min1}, R_{min2}\}$$

$$R_{min1} = \begin{cases} |c(0)| & \text{if } \mathrm{Re}(\Lambda(\omega_f)) \leq -\frac{2h}{\pi K_c} \\ \left|\Lambda(\omega_f) + \frac{2h}{K_c}\right| & \text{if } \mathrm{Re}(\Lambda(\omega_f)) > -\frac{2h}{\pi K_c} \end{cases}$$

$$R_{min2} = \max_{t\in(0,T_f/2)} \frac{c(t) - Cz(0)\cos\omega_f t}{\sin\omega_f t}$$

$\Lambda(.)$ is the Tsypkin locus and K_c is the critical gain of $G(s)$. $c(0)$ and $z(0)$ are the plant output and state vector corresponding to the positive switch of the relay at steady state.

Proof. See Chapter 2. □

As mentioned in the previous chapter, a Tsypkin locus is defined as :

$$\Lambda(\omega_f) \triangleq \frac{1}{\omega_f}\dot{c}(0, T_f) + jc(0, T_f).$$

R_{min1} and R_{min2} are both finite and it follows that if $R \geq R_{min}$, FO is guaranteed to occur in the RFS. Therefore, for a sinusoidal dither, FO can always be enforced in the RFS if R is sufficiently large.

3.3 Identification of T_f^*

Regardless of the dither shape, when the RFS undergoes steady state oscillations of frequency $\omega_f = 2\pi/T_f$, the input to the linear element, $G(s)$, is a square wave with period, T_f. The response of $G(s)$ is also periodic with maximum amplitudes which are dependent on the amplitude and frequency of the input square wave. The relationship between the maximum amplitudes and the frequency of the input signal is nonlinear. It is conceivable that for $G(s)$ with multiple lightly damped modes, one can expect that the function of maximum output amplitudes with respect to the frequency of the input square wave will exhibit several local maxima as shown in Figure 3.2, simulated for $G(s) = 1000/(s^5+6s^4+58s^3+211s^2+629s+471)$. In this example, $T_f^* = 1.04$ is identified to be the first peak in Figure 3.2 since for all frequencies above $f_{min} = 2\pi/T_f^*$ the amplitude of the output of $G(s)$ decreases steadily.

In this section, a simple approach is proposed for finding T_f^*. We begin by assuming that the dither signal is able to generate FO in the loop which is of the same frequency as the dither. This assumption follows from Proposition 3.1.

Thus consider the steady state plant output, $c(t, T_f)$ for an input square wave

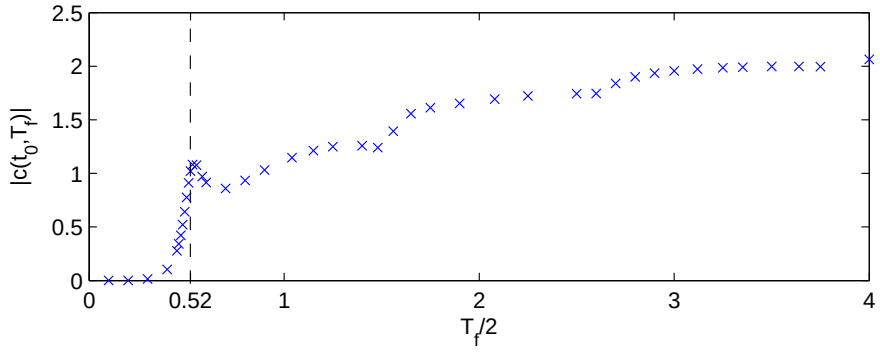

Fig. 3.2. Plot of the amplitude of oscillation against $T_f/2$ for $G(s) = 1000/(s^5 + 6s^4 + 58s^3 + 211s^2 + 629s + 471)$.

with period T_f where

$$c(t, T_f) = Ce^{At}z(0) + \int_0^t e^{A(t-\tau)}Bhd\tau \tag{3.5}$$

$$z(0) = -(I + e^{A\frac{T_f}{2}})^{-1}(2e^{A(\frac{T_f}{2}-(L-n\frac{T_f}{2}))} - e^{A(\frac{T_f}{2})} - I)(-1)^n A^{-1}Bh. \tag{3.6}$$

It follows that

$$\dot{c}(t, T_f) = C(Az(t) + Bu(t - L)).$$

Since this is a steady state analysis, time $t = 0$ is chosen to correspond to the positive switching edge of the relay. Furthermore, the above formulation is written for the general case when $n\frac{T_f}{2} < L \leq (n+1)\frac{T_f}{2}$ where $n = floor(\frac{2L}{T_f})$.

Suppose the maximum amplitude of $c(t, T_f)$ occurs at $t = t_0$ where

$$t_0(T_f) = \arg\max_{t \in R} c(t, T_f). \tag{3.7}$$

The peak amplitude occurring at $t = t_0$ can be written as :

$$c(t_0, T_f) = Ce^{At_0}z(0) + C(e^{At_0} - I)A^{-1}Bh. \tag{3.8}$$

To further determine the peak amplitude with respect to T_f, differentiate $c(t_0, T_f)$ with respect to T_f as follows :

$$\frac{dc(t_0,T_f)}{dT_f} = Ce^{At_0}Az(0)\frac{dt_0}{dT_f} + Ce^{At_0}\frac{dz(0)}{dT_f} + Ce^{At_0}Bh\frac{dt_0}{dT_f} \tag{3.9}$$

Equating (3.9) to zero, the turning points of $c(t_0, T_f)$ with respect to T_f can be obtained either analytically or numerically. The set $(0, T_f^*)$ where the amplitude of oscillation decreases monotonically with T_f can then be identified. This is shown in Figure 3.3 for a plant with transfer function $G(s) = \frac{1}{s^2+2s+20}$ where $T_f^* = 1.4414$.

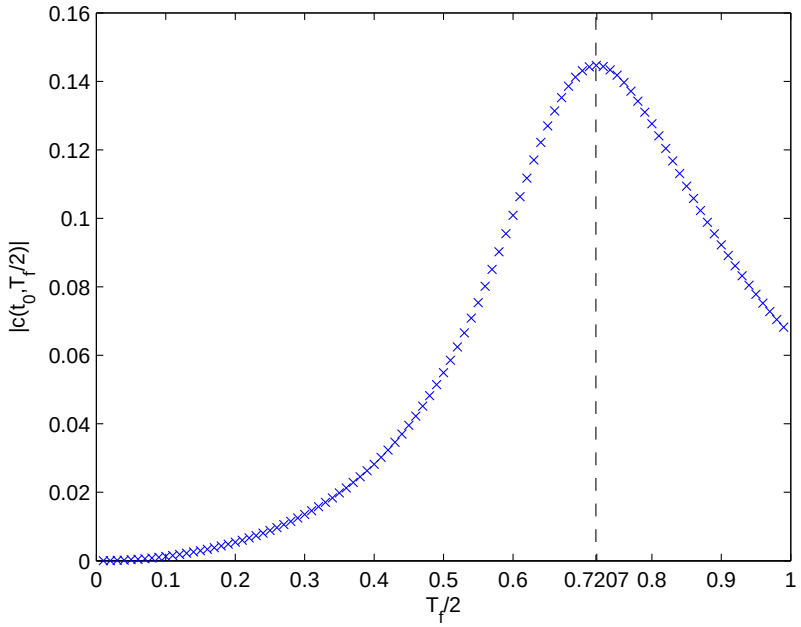

Fig. 3.3. Plot of the amplitude of oscillation against $T_f/2$ for $G(s) = \frac{1}{s^2+2s+20}$.

Remark 3.1. It should be noted that $\dot{c}(t, T_f)$ is continuous except for $G(s)$ with relative degree one. In such cases, the discontinuities occur at $t = L - n\frac{T_f}{2}$ following a relay switch, like in Figure 2.4. Thus the maximum output also occurs at $t_0 =$

$L - n\frac{T_f}{2}$. Hence for such systems, the maximum output, $c(t_0, T_f)$, can be completely written.

Remark 3.2. The minimum amplitude, R_{min} of the sinusoidal dither that can enforce FO in the RFS is determined by Proposition 3.1.

For non-sinusoidal dithers, FO can also be enforced if the magnitude is arbitrarily large. As long as FO is achieved, the relay switches with an amplitude of h and $c(t, T_f)$ is independent of the dither shape. This also implies that T_f^* is independent of the exact dither signal shape. This is a significant breakthrough because T_f^* applies to all periodic dithers of any shape. This is further discussed in Section 3.6. In much of the current literature, results have only been for very specific dither shapes and furthermore, their analyses have mostly been approximate, in many cases using averaging to achieve their approximate results(Luigi Iannelli, 2003*a*; Luigi Iannelli, 2003*b*; Brad Lehman, 1996).

The solution to $\frac{c(t_0,T_f)}{dT_f} = 0$ is not a trivial one and can only be solved for simple $G(s)$, as will be shown in Section 3.5. For higher order plants, it is generally inconvenient to solve this numerically. In the next section, we will show how the generalized Tsypkin Locus can be used to graphically determine T_f^* and $c(t_0, T_f^*)$.

3.4 Solution of T_f^* using the Generalized Tsypkin Locus

The Tsypkin locus (Tsypkin, 1984) is one approach that has been used to solve for the existence of limit cycles in a RFS. It is an exact method which has been used extensively in (Lim *et al.*, 2005) to find the minimum conditions for forced oscillations to occur in a RFS. However in this chapter, we require the generalized Tsypkin locus defined as :

$$\Lambda(t, \omega_f) \triangleq \frac{1}{\omega_f}\dot{c}(t, T_f) + jc(t, T_f).$$

Thus a generalized Tsypkin locus is a three dimensional plot involving $(t, c, \dot{c})$ and parameterized by the frequency, ω_f. The conventional Tsypkin locus is a special case where $t = 0$.

In the problem formulation for the identification of T_f^*, there are 2 unknowns, t_0 and T_f^*. Suppose a series of generalized Tsypkin loci is plotted for different values of t. For each t, the Tsypkin locus may cut the c- and $\dot{c}$-axes a number of times. Each of the crossings at the c-axis represents a turning point ($\dot{c}(t, T_f) = 0$) of $c(t, T_f)$ for the dither signal of period T_f. If several Tsypkin loci for different t are examined at the c-axis for the same T_f, the result is a series of turning points of $c(t, T_f)$ corresponding to FO at T_f. Accordingly, the maximum value of $|c(t, T_f)|$ (denoted as $|c(t_0, T_f)|$) can thus be located. If this process is extended for different T_f, the maximum of $|c(t_0, T_f)|$ over all T_f can likewise be identified. Thus, T_f^* is also determined. This method is demonstrated in the following example.

Example 3.1. Consider a fourth order plant with transfer function, $G(s) = \frac{1}{s^4+6s^3+23s^2+20s+26}$, with complex roots at $s = -2.657 \pm 3.2928i$ and $s = -0.343 \pm 1.1553i$. A series of Tsypkin Loci, $c(t, T_f)$ against $\dot{c}(t, T_f)/\omega_f$ is plotted for $t = 0.05, 0.1, 0.15, 0.2049, 0.25, 0.3$, as shown in Figure 3.4. It can be seen that the maximum $|c(t, T_f)|$ is 0.0893 and it occurs at $t = 0.2049 = t_0$. The intersection of the Tsypkin locus, $c(0.2049, T_f)$ vs $\dot{c}(0.2049, T_f)$ with the plane $\dot{c}(t, T_f)/\omega_f = 0$ is $T_f = 2.76$. This gives $T_f^* = 2.76$.

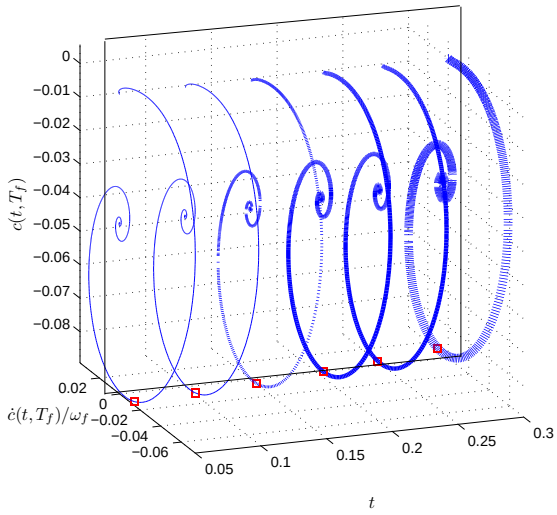

Fig. 3.4. Plot of the generalized Tsypkin Locus in example 3.1.

In the following section, some closed form solutions for T_f^* for a number of special cases are presented.

3.5 Special Cases

Proposition 3.2. *For first order plants with delay, $c(t_0, T_f)$ increases monotonically with respect to T_f. Also, $T_f^* = \infty$ and $t_0(T_f) = L - nT_f/2$ for $n = floor(\frac{2L}{T_f})$. It also follows that $\lim_{T_f \to 0} c(t_0, T_f) = 0$.*

Proof. In first order systems with delay, at steady state, $c(t, T_f)$ should be written in two parts due to the discontinuity resulting from the delay :

$$c_1(t, T_f) = Ce^{At}z(0) + C(e^{At} - I)A^{-1}Bh(-1)^{n+1} \quad t \in [0, L - n\frac{T_f}{2}] \tag{3.10}$$

$$c_2(t, T_f) = Ce^{At}z(0) + C(2e^{A(t-L+n\frac{T_f}{2})} - e^{At} - I)A^{-1}Bh(-1)^{n} \quad t \in [L - n\frac{T_f}{2}, \frac{T_f}{2}] \tag{3.11}$$

where $z(0)$ is given in (3.6) and $n = floor(\frac{2L}{T_f})$. It is assumed that the initial condition $z(0)$ corresponds to the positive switching edge of the relay at steady state. It follows that

$$\dot{c}_1(t, T_f) = Ce^{At}Az(0) + Ce^{At}Bh(-1)^{n+1} \quad t \in (0, L - n\frac{T_f}{2}] \tag{3.12}$$

$$\dot{c}_2(t, T_f) = Ce^{At}Az(0) + C(2e^{A(t-L+n\frac{T_f}{2})} - e^{At})Bh(-1)^{n} \quad t \in [L - n\frac{T_f}{2}, \frac{T_f}{2}] \tag{3.13}$$

Note that $z(0)$ is positive (negative) when n is odd (even) and $|Ce^{At}Az(0)| < |Ce^{At}Bh|$. Accordingly, $\dot{c}_1(t, T_f)$ is positive (negative) when n is odd (even) while $\dot{c}_2(t, T_f)$ is negative (positive) for the same n. This implies that $c(t, T_f)$ is either increasing or decreasing monotonically in each time segment and the maximum

amplitude occurs at $t = L - nT_f/2 = t_0$. This maximum is given by :

$$\begin{aligned}
&|Cz(L - n\frac{T_f}{2}, T_f)| \\
&= |Ce^{A(L-n\frac{T_f}{2})}z(0) + C(I - e^{A(L-n\frac{T_f}{2})})(-1)^n A^{-1}Bh| \\
&= |C(I - 2e^{A\frac{T_f}{2}}(I + e^{A\frac{T_f}{2}})^{-1})A^{-1}Bh| \\
&= |C(\frac{I - e^{A\frac{T_f}{2}}}{I + e^{A\frac{T_f}{2}}})A^{-1}Bh| \to 0 \text{ as } T_f \to 0 \text{ and } A \text{ is Hurwitz.}
\end{aligned} \tag{3.14}$$

□

Remark 3.3. For such plants, any self-oscillations can be quenched or reduced easily by an external dither signal with a frequency higher than that of the self-oscillations.

Example 3.2. Consider $G(s) = \frac{e^{-s}}{s+1}$. The undithered and dithered RFS of period $T_f = 0.8$ and 0.3 are plotted in Figure 3.5. It can be seen that the amplitude of the dithered system is smaller than that of the undithered case. The minimum amplitude of the dither signal required to produce the desired oscillations are $R = 0.54, 0.38$ for $T_f/2 = 0.8, 0.3$ respectively. Figure 3.6 plots the amplitude of the oscillation for a range of periods of the dither signal. From the figure, it can be seen that the smaller the period of the dither signal, the smaller is the amplitude of oscillations in the RFS.

Proposition 3.3. *For second order plants with distinct (λ_1, λ_2) and repeated (λ_1) roots, $c(t_0, T_f)$ increases monotonically with respect to T_f. Also $T_f^* = \infty$ and*

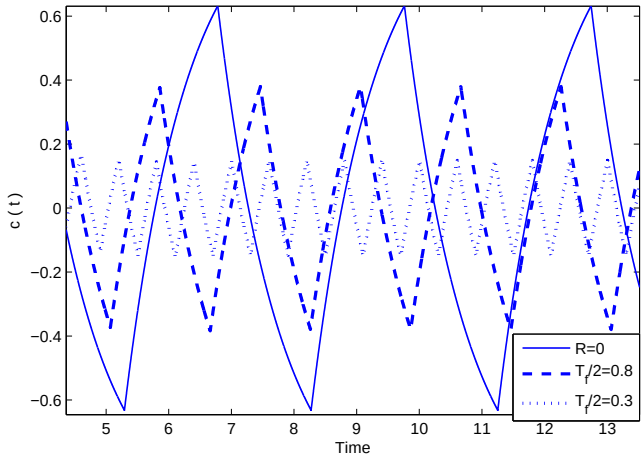

Fig. 3.5. Self oscillation and FO of differing $T_f/2$ in example 3.2.

(i) for distinct roots, $t_0(T_f) = \frac{1}{\lambda_1-\lambda_2} \ln\left(\frac{\tanh(0.25\lambda_2 T_f)-1}{\tanh(0.25\lambda_1 T_f)-1}\right)$ *and* $t_0(T_f^*) = \lim_{T_f\to 0} t_0(T_f) = 0$.

(ii) for repeated roots, $t_0(T_f) = \frac{0.5T_f}{-\sinh(0.5\lambda_1 T_f)+1+\cosh(0.5\lambda_1 T_f)}$ *and* $t_0(T_f^*) = \lim_{T_f\to\infty} t_0(T_f) = T_f/2$.

In addition, $\lim_{T_f\to 0} c(t_0, T_f) = 0$.

Proof. For a second order system with repeated roots at λ_1, its state space representation is $A = [0\ 1;\ -\lambda_1^2\ 2\lambda_1]$, $b = [0\ 1]^T$, $c = [1\ 0]$ where $\lambda_1 < 0$. The states of $z(0)$ are given by $z_1(0) = \frac{-0.5\lambda_1 T_f+\sinh(\lambda_1 T_f)}{\lambda_1^2(1+\cosh(0.5\lambda_1 T_f))}$ and $z_2(0) = -\frac{0.5T_f}{1+\cosh(0.5\lambda_1 T_f)}$.

Equating $\frac{dc(t_0,T_f)}{dt_0}$ to zero,

$$\begin{aligned} t_0 &= \frac{-z_2(0)}{z_2(0)\lambda_1 - \lambda_1^2 z_1(0) + 1} \\ &= \frac{0.5T_f}{-\sinh(0.5\lambda_1 T_f) + 1 + \cosh(0.5\lambda_1 T_f)} > 0. \end{aligned} \tag{3.15}$$

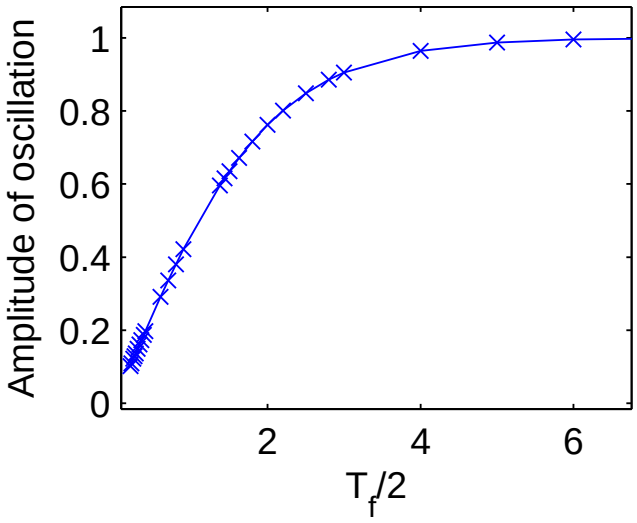

Fig. 3.6. Plot of the amplitude of oscillation against $T_f/2$ in example 3.2.

The change in the output amplitude w.r.t. T_f,

$$\begin{aligned}\frac{dc(t_0,T_f)}{dT_f} &= Ce^{At_0}\frac{dz(0)}{dT_f} \\ &= e^{\lambda_1 t_0}(\frac{dz_1(0)}{dT_f} - \lambda_1 t_0\frac{dz_1(0)}{dT_f} + t_0\frac{dz_2(0)}{dT_f}). \end{aligned} \tag{3.16}$$

The factor in (3.16),

$$\begin{aligned}&\frac{dz_1(0)}{dT_f} - \lambda_1 t_0\frac{dz_1(0)}{dT_f} + t_0\frac{dz_2(0)}{dT_f} \\ =\ &\frac{0.5T_f\sinh(0.5\lambda_1 T_f)}{(1+\cosh(0.5\lambda_1 T_f))^2} + t_0(-\frac{1}{\cosh(0.5\lambda_1 T_f)}) < 0\end{aligned}$$

which implies that the output $c(t_0,T_f)$ is monotonically decreasing and the amplitude $|c(t_0,T_f)|$ increases with T_f. Thus, similar to the first order case, $T_f^* = \infty$. For (3.15), the factor $-\sinh(0.5\lambda_1 T_f) + 1 + \cosh(0.5\lambda_1 T_f)$ decreases to 0 exponentially as T_f tends to ∞ and $\lim_{T_f\to\infty} t_0 = 0.5T_f$.

For a second order plant with distinct real roots, its state space representation in controllable canonical form is $A = [0\ 1;\ -\lambda_1\lambda_2\ \ (\lambda_1+\lambda_2)]$, $B = [0\ 1]^T$ and

$C = [1\ 0]$ where $\lambda_1 < \lambda_2 < 0$ are the roots of the plant.

A closed form solution for t_0 is

$$t_0 = \frac{1}{\lambda_1 - \lambda_2} \ln\left(\frac{\lambda_1\lambda_2 z_1(0) - \lambda_2 z_2(0) - 1}{\lambda_1\lambda_2 z_1(0) - \lambda_1 z_2(0) - 1}\right) > 0. \tag{3.17}$$

The change in the output amplitude w.r.t. T_f,

$$\frac{dc(t_0, T_f)}{dT_f} = \mathrm{e}^{\lambda_1 t_0}\left(\lambda_2 \frac{dz_1(0)}{dT_f}\right) + \mathrm{e}^{\lambda_2 t_0}\left(\frac{dz_2(0)}{dT_f} - \lambda_1 \frac{dz_1(0)}{dT_f}\right) \tag{3.18}$$

where $z_1(0) = \frac{-\lambda_2 \tanh(0.25\lambda_1 T_f) + \lambda_1 \tanh(0.25\lambda_2 T_f)}{\lambda_1^2\lambda_2 - \lambda_1\lambda_2^2}$ and $z_2(0) = \frac{-\tanh(0.25\lambda_1 T_f) + \tanh(0.25\lambda_2 T_f)}{\lambda_1 - \lambda_2}$ are the states of $z(0)$ and $t_0 = \frac{1}{\lambda_1 - \lambda_2} \ln\left(\frac{\tanh(0.25\lambda_2 T_f) - 1}{\tanh(0.25\lambda_1 T_f) - 1}\right)$.

In (3.18),

$$\lambda_2 \frac{dz_1(0)}{dT_f} = 0.5\mathrm{sech}(0.25\lambda_1 T_f) > 0$$

and

$$\frac{dz_2(0)}{dT_f} - \lambda_1 \frac{dz_1(0)}{dT_f} = -0.5\mathrm{sech}(0.25\lambda_2 T_f) < 0.$$

Thus from (3.18),

$$\frac{dc(t_0, T_f)}{dT_f} < 0 \text{ since } \lambda_1 < \lambda_2 < 0.$$

Hence the output $c(t_0, T_f)$ ($|c(t_0, T_f)|$) decreases (increases) monotonically with increasing T_f. Once again, $T_f* = \infty$. For (3.17), as T_f tends to ∞, t_0 tends to 0. □

Example 3.3. Consider $G(s) = \frac{1}{s^2+5s+6}$, with poles at $\lambda_1 = -2$ and $\lambda_2 = -3$. The Tsypkin Locus is shown in Figure 3.7(a). The magnitude of $c(T_f/2, T_f)$ increases as $T_f/2$ increases and saturates at $c(T_f/2, T_f) = -0.1667$ when $T_f^* = \infty$. The amplitude of the oscillation is plotted against $T_f/2$ in Figure 3.7(b). From the figure,

it can be seen that the larger the period of oscillation, the larger the amplitude $|c(t_0, T_f)|$.

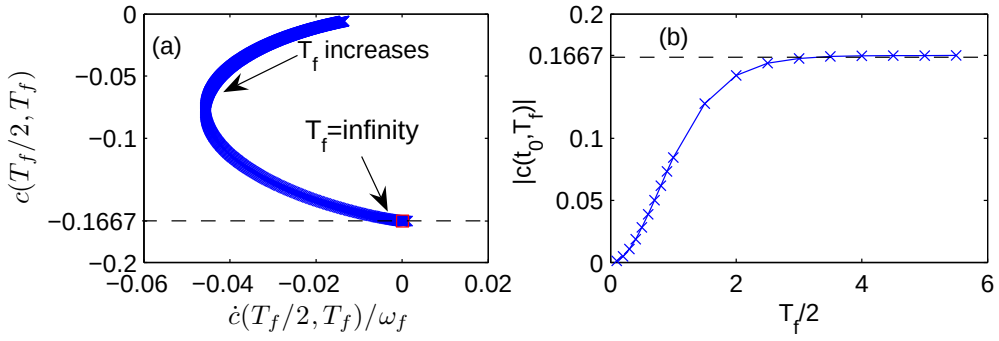

Fig. 3.7. (a)Plot of the Tsypkin Locus in example 3.3. (b)Plot of the amplitude of oscillation against $T_f/2$ in example 3.3.

Proposition 3.4. *For second order plants with complex roots* $a \pm jb$, $c(t_0, T_f)$ *increases monotonically for* $T_f \in (0, T_f^*)$ *where* $T_f^* = \frac{\pi}{b}$. *Also,* $t_0(T_f) = \frac{1}{b}\tan^{-1}(\frac{bz_2(0)}{(a^2+b^2)z_1(0)-az_2(0)-1})$ *where* $z_1(0) = \frac{-asin(bT_f)+bsinh(aT_f)}{b(a^2+b^2)(cos(bT_f)+cosh(aT_f))}$ *and* $z_2(0) = \frac{-sin(bT_f)}{b(cos(bT_f)+cosh(aT_f))}$. *It follows that* $t_0(T_f^*) = \frac{\pi}{b}$.

Proof. For a second order plant with complex roots, $a \pm jb$, its state space representation can be written as $A = [0\ 1;\ -(a^2+b^2)\ 2a]$, $B = [0\ 1]^T$, $C = [1\ 0]$ and the turning point t_0 of the output is given by

$$t_0 = \frac{1}{b}\tan^{-1}(\frac{bz_2(0)}{(a^2+b^2)z_1(0) - az_2(0) - 1}) \tag{3.19}$$

where $z_1(0) = \frac{-asin(bT_f)+bsinh(aT_f)}{b(a^2+b^2)(cos(bT_f)+cosh(aT_f))}$ and $z_2(0) = \frac{-sin(bT_f)}{b(cos(bT_f)+cosh(aT_f))}$.

For $t = t_0$, the output amplitude for varying T_f is given by (3.8). The bound T_f^* where the amplitude of oscillation $c(t_0, T_f)$ decreases monotonically with T_f for

the set $(0, T_f^*)$ is determined by equating (3.9) to zero, which gives

$$Ce^{At_0}\frac{dz(0)}{dT_f} = 0. \tag{3.20}$$

Solving (3.20) gives $\frac{T_f}{2} = \frac{m\pi}{b}$ where $m \in N^+$. Thus, for a second order system with complex roots, the amplitude of the limit cycle decreases monotonically with decreasing period for $T_f \in (0, T_f^*)$ where $T_f^* = \frac{2\pi}{b}$ and the corresponding $t_0 = \frac{\pi}{b}$.

□

Example 3.4. Consider a second order plant with transfer function, $G(s) = \frac{1}{s^2+2s+20}$, with complex roots at $s = -1 \pm 4.36j$. The Tsypkin Locus in Figure 3.8(a) shows that the outer spiral with $c(T_f/2, T_f)$ increases in magnitude from zero to about 0.15 before spiralling in with lower magnitudes. Hence the maximum T_f corresponding to maximum magnitude can be determined by the point which crosses the c-axis or the point corresponding to $\dot{c}(T_f/2, T_f) = 0$. This gives $T_f^*/2 = 0.7207$. The amplitude of the oscillation is plotted against the period of oscillation in Figure 3.8(b) which verifies the results obtained from the Tsypkin Locus. From the figure, it can be seen that for $T_f^*/2 = 0.7207$, the maximum amplitude is about 0.15.

3.6 Quenching with Other Dither Signals

In this section, we show that the T_f^* obtained for the sinusoidal dither remains valid in the same RFS when dithers of other shapes are applied. This is an interesting and new discovery as it means that quenching is now possible for any kind of

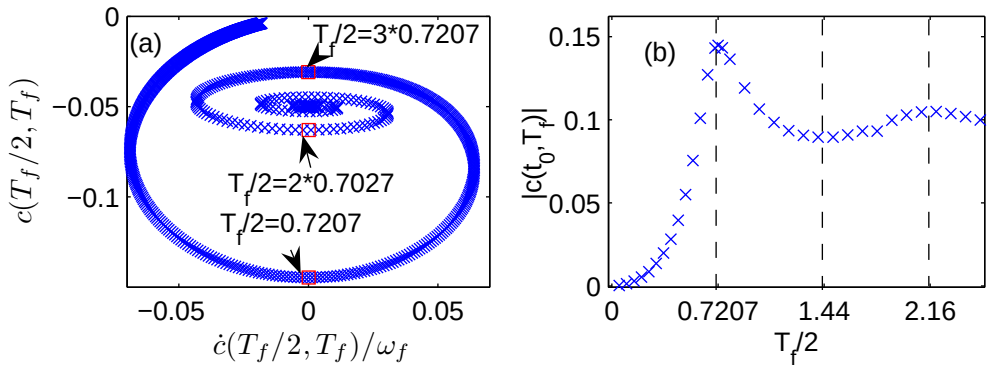

Fig. 3.8. (a)Plot of the Tsypkin Locus in example 3.4. (b)Plot of the amplitude of oscillation against $T_f/2$ in example 3.4.

periodic signal in a RFS. The results are only dependent on the linear element in the RFS.

Consider the second order plant with transfer function, $G(s) = \frac{1}{s^2+2s+20}$ in Example 3.4 with an external triangular dither signal. The amplitude of the oscillation is plotted against the period of oscillation in Figure 3.9(a) which shows that $T_f^*/2 = 0.7207$ and verifies the results in Section 3.5. At $T_f/2 = 0.7207$, $u(t)$, $c(t)$ and $f(t)$ are plotted in Figure 3.9(b). It can be checked from the figure that $\dot{c}(T_f/2, 1.4415) = 0$ and the maximum amplitude is about 0.15.

For the same RFS as above, consider a composite dither which is a combination of two sinusoids. If this dither has a sufficiently large amplitude to achieve FO at the fundamental frequency of the composite dither, the same T_f^* applies. The composite dither is shown in Figure 3.10(b). The plot of $c(t_0, T_f)$ against $T_f/2$ shown in Figure 3.10(a) is identical to that of Figure 3.9(a). The resulting $c(t, T_f^*)$ is also identical to Figure 3.9(b).

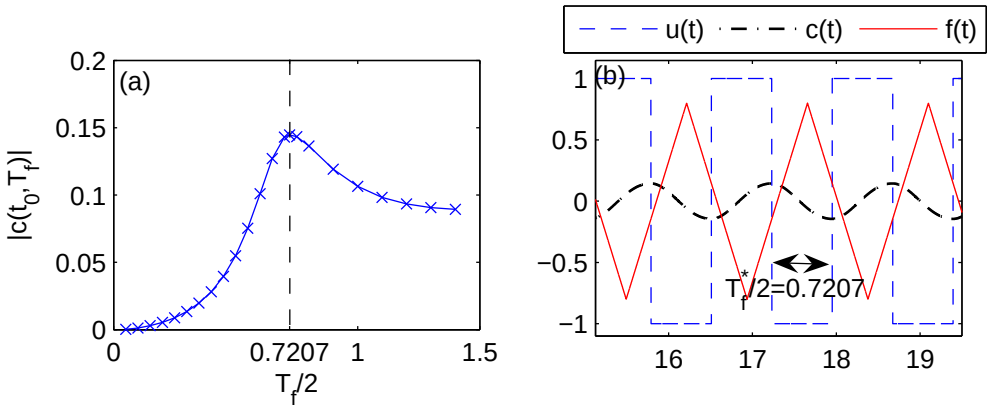

Fig. 3.9. (a) Maximum oscillation amplitudes with triangular dithers. (b) Plot of $u(t)$, $c(t)$ and $f(t)$ for $T_f/2 = 0.7207$.

3.7 Applications

In this section, the analysis of two motivating examples will be presented and a comparison between the performance of different dither shapes will be carried out.

Example 3.5. The following problem is posed by (Gibson, 1963), converted to SI units by (Taylor, 2000) and adapted to illustrate our problem. A common problem in the control of a missile is the limitation of the tendency of the missile to roll, or spin about its axis. Aerodynamic surfaces are considered undesirable and difficult to design due to the change in air density experienced by the missile and would be ineffective except for the short time the missile is in the atmosphere. A common solution is to mount a pair of control jet on the missile, one to produce torque about the roll axis in the clockwise sense and one in the counterclockwise sense. The force exerted by each jet is $F_0 = 445N$ and the moment arms are $R_0 = 0.61m$. The moment of inertia about the roll axis is $J = 4.68N \cdot m/s^2$. Let the control jets and

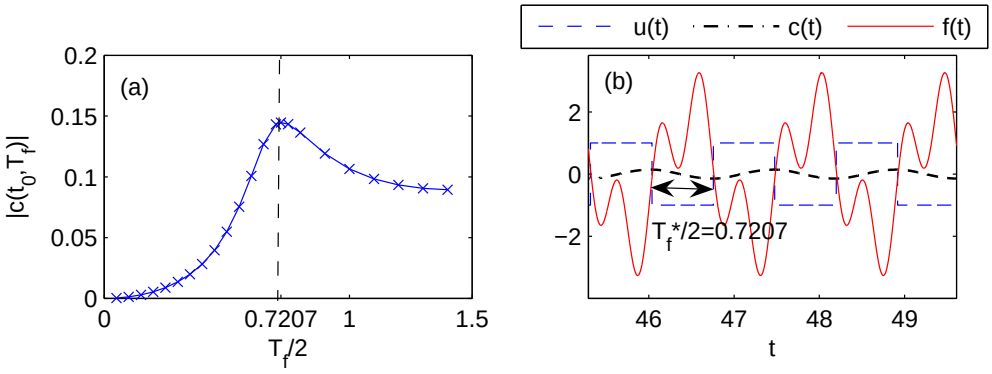

Fig. 3.10. (a)Maximum oscillation amplitudes with composite sinusoidal dithers. (b)Plot of $u(t)$, $c(t)$ and $f(t)$ for $T_f/2 = 0.7207$.

associated servo actuator have a hysteresis $h = 22.24N$ and two lags corresponding to time constants of $0.01s$ and $0.05s$. To control the roll motion, there is roll and roll rate feedback with gains of $K_p = 1868N/radian$ and $K_v = 186.8N \cdot /radian$ respectively. The block diagram is shown in Figure 3.11. The self oscillation and dithered response are shown in Figure 3.12 where $T_f/2 = 0.037$ and amplitude of 0.55. It can be verified that the oscillations are indeed reduced. Figure 3.13 plots $c(t, T_f)$ with sinusoidal dither and sawtooth dither where $T_f/2 = 0.037$. It can be seen that the oscillation amplitudes are the same in both cases.

Example 3.6. Consider the case of a DC motor whose model is given in Figure 3.14 (adapted from (Luigi Iannelli, 2003*b*)). The DC motor is modeled as an electric (armature) circuit subsystem with a given armature resistance R_a and inductance L_a and a mechanical subsystem with inertia J and viscous coefficient β. The motor provides a torque proportional to the armature current i_a through the torque constant k_t and a counter electromagnetic force proportional to the rotor

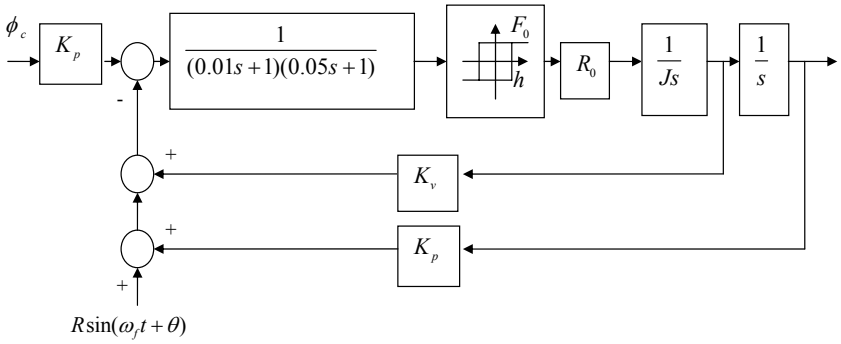

Fig. 3.11. Block diagram of the Missile Roll-Control problem. (Taylor, 2000)

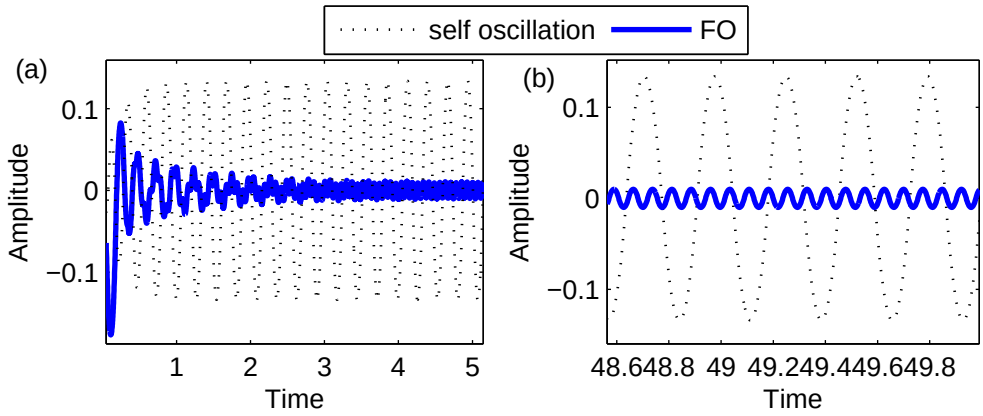

Fig. 3.12. (a)Comparison of the oscillation amplitudes in example 3.5. (b)Comparison of the steady state oscillation amplitudes in example 3.5.

speed through the constant k_e. The angular position of the shaft θ is measured by using a rotational potentiometer whose gain is k_{pot}. The motor supply voltage is $\pm V_a$ and is obtained through a full bridge DC/DC converter (H-bridge). This power amplifier has a logic input that selects a positive or negative supply voltage to the DC motor. The control loop is closed by feeding in the negative of the sum of the position and the dither signal. The output of the relay is the input of the

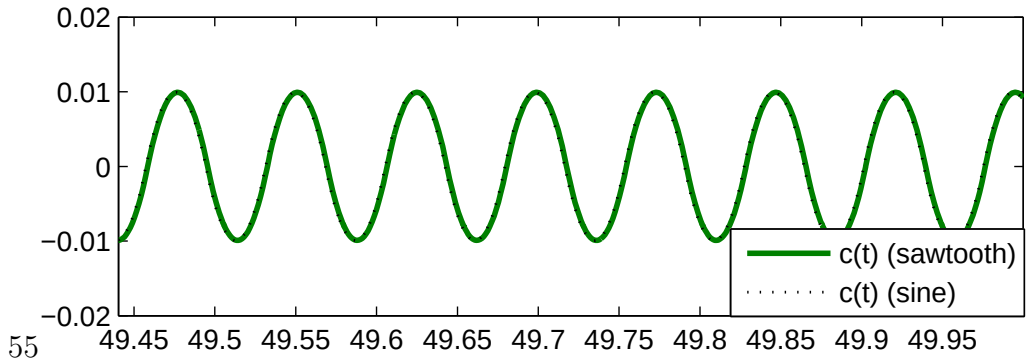

55

Fig. 3.13. Plot of $c(t)$ with sinusoidal and sawtooth dithers.

H-bridge driver. By introducing the state vector $x = \begin{bmatrix} \theta \\ \omega \\ i_a \end{bmatrix}$, we have

$$\dot{x}(t) = \begin{bmatrix} 0 & 1 & 0 \\ 0 & -\frac{\beta}{J} & \frac{k_t}{J} \\ 0 & -\frac{k_e}{L_a} & -\frac{R}{L_a} \end{bmatrix} x(t) \pm \begin{bmatrix} 0 \\ 0 \\ \frac{V_a}{L_a} \end{bmatrix}, \; C = [-k_{pot}\ 0\ 0]$$

The closed loop transfer function is

$$\frac{k_t k_{pot} V_a L}{JLL_a s^3 + (\beta L + R_1 J)L_a s^2 + (\beta R_1 + k_t k_e)L_a s}.$$

The system exhibited self oscillation, FO and SO with the following set of parameters. $V_a = 5V$, $R_1 = 2.510\Omega$, $L_a = 0.530mH$, $k_t = k_e = 5.700mV/rad \cdot s^-1$, $\beta = 0.411mN \cdot cm/rad \cdot s^-1$, $J = 31.400g \cdot cm^2$, $k_{pot} = 3/2\pi V/rad$, $Tf/2 = 0.005$ and amplitude 0.05. It is shown in Figure 3.15 that the amplitudes of the oscillations are indeed reduced with a dither frequency higher than that of self oscillation. Figure 3.16 plots the oscillation amplitudes for a sine dither and a sawtooth dither where the dither amplitudes are 0.07 and frequencies at 100 Hz. It can be seen that the oscillation amplitudes are the same in both cases.

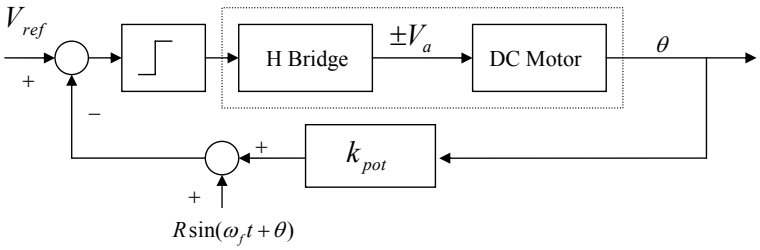

Fig. 3.14. Model of the DC motor in example 3.6.

3.8 Conclusion

In this chapter, the potential of using a dither in arbitrarily reducing inherent system oscillations has been illustrated. The bound on the dither period, T_f^* was determined and shown to be independent of the dither shape. The analysis is exact and results can be obtained from the generalized Tsypkin Loci. For first and second order real plants, it was shown that $T_f^* = \infty$ which implies that quenching can be achieved with arbitrarily small amplitudes.

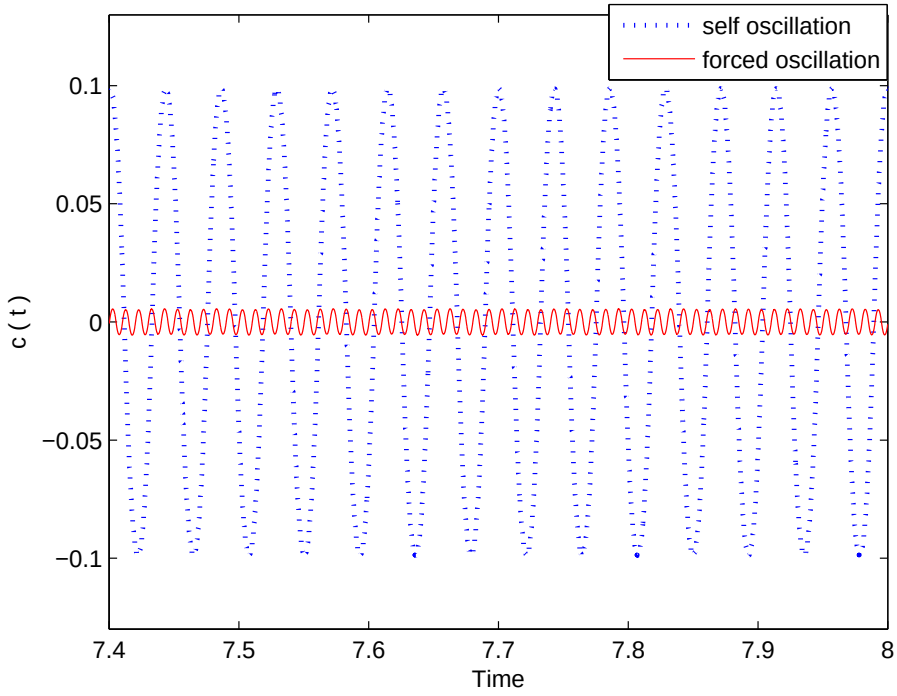

Fig. 3.15. Comparison of the oscillation amplitudes of the DC motor in example 3.6.

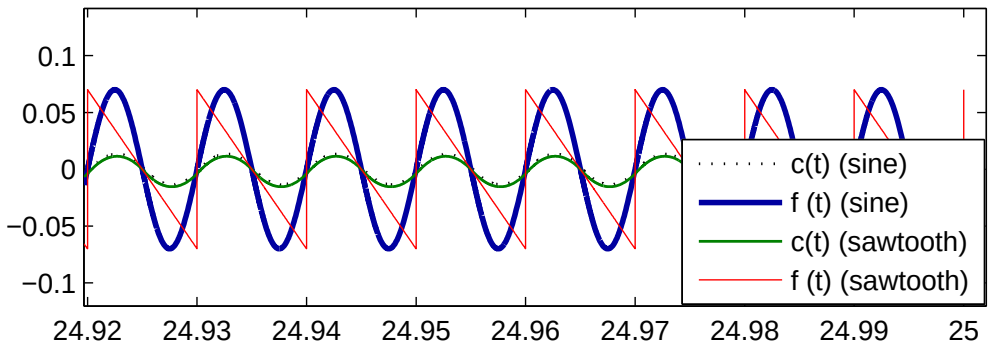

Fig. 3.16. Comparison of the oscillation amplitudes between the sinusoidal and sawtooth dithers in example 3.6.

Chapter 4

Limit Cycles in Quantized Feedback Systems under High Quantization Resolution

4.1 Introduction

In Chapters 2 and 3, we have given necessary and sufficient conditions for the existence of forced and subharmonic oscillations in relay feedback systems. In this chapter, we extend the periodic switching conditions in Chapter 2 to analyse the existence of self oscillations in certain quantized feedback systems under high quantization resolution (small quantization step size) and no external forcing signals. Like the relay in Chapter 2, the output of the quantizer is discontinuous at its switching instants. However, the quantizer is a more general nonlinearity as compared to the relay, due to its switchings at multiple discrete levels. Due to

their switching nature, the relay and the quantized feedback systems share some similarities in terms of behaviours like self oscillations. Similar to the relay feedback system, the quantized feedback system will self oscillate when the necessary and sufficient conditions are satisfied, like in Chapter 2.

An evaluation of the extended periodic switching conditions in Chapter 2 uncovers the existence of self oscillations for some, but not all systems under high quantization resolution. In particular, we show that multiple limit cycle solutions of the switching instants and period can be obtained, depending on the initial states of the system. Further analysis on the stability of the limit cycle via the Jacobian of the Poincaré map reveals numerical bounds on the quantization step size. In some cases, the limit cycle is found to be stable for quantization step size as small as 0.005.

This chapter is structured as follows. The problem formulation is discussed in Section 4.2. In Section 4.3, the analysis on the necessary conditions for the existence and stability of limit cycles are shown. Further results on the identification of the bounds on the quantization step size are presented in Section 4.3.3. Conclusions are given in Section 4.4.

4.2 Problem Formulation

Consider the quantized feedback system in Figure 4.1 with a finite limit midtread quantizer $Q_\Delta(x)$. The linear system, $G(s)$, is assumed to have a state space description given by

$$\begin{aligned} \dot{z}(t) &= Az(t) + Bu(t) \\ c(t) &= Cz(t) \end{aligned} \tag{4.1}$$

with

$$u = j\Delta,\ (j-0.5)\Delta < x \leq (j+0.5)\Delta \tag{4.2}$$

$$|u| \leq M,\ x > M + 0.5\Delta or x \leq -M - 0.5\Delta \tag{4.3}$$

where $j \in \mathbb{Z}$, $u, c \in \mathbb{R}$ are the input and output, respectively, $z \in \mathbb{R}^{m\times 1}$ is the state vector, $A \in \mathbb{R}^{m\times m}$ is Hurwitz and assumed to be non-singular, $B \in \mathbb{R}^{m\times 1}$, $C \in \mathbb{R}^{1\times m}$, $M, \Delta \in \mathbb{R}$ are the saturation limit and step size of the quantizer respectively and $x(t) = -c(t)$ where $x(t)$ is the feedback error. We define the quantizer, $Q(.) = Q_\Delta(x)$ by the formula

$$Q_\Delta(x) = \begin{cases} M, & if\ x > M + 0.5\Delta \\ -M, & if\ x \leq -M - 0.5\Delta \\ \lfloor \frac{x}{\Delta} + 0.5 \rfloor \Delta, & if\ -M - 0.5\Delta < x \leq M + 0.5\Delta \end{cases} \tag{4.4}$$

where $\Delta = 2M/(k-1)$ for k being the number of quantization levels. This is illustrated in Figure 4.2 for the quantizer with $\Delta = 5$ and $M = 10$.

In order to maintain a constant saturation limit, we preset the quantization step size Δ as $\Delta = 2M/(k-1)$ where k is the number of quantization levels and

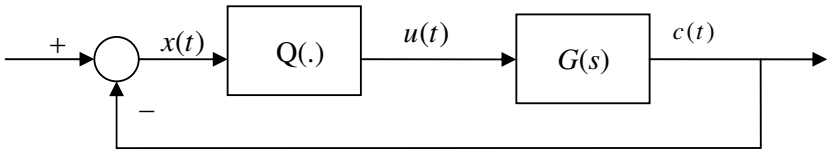

Fig. 4.1. Quantized feedback system.

refer to the quantization resolution as an inverse function of the step size, Δ. Thus, it is expected that as the number of quantization level k increases, the quantization step size Δ will decrease and result in a higher quantization resolution. Thus as the quantization step size decrease, the slope of the quantizer will decrease.

It is also required that the system in Figure 4.1 is asymptotically stable when $Q(.) = 1$. This forms the basis of our study for self oscillations when $Q(.)$ is replaced by a quantizer. When $Q(.)$ is an uniform quantizer the self oscillations that it may induce in the system is then examined. This self oscillation may be induced by non-zero initial conditions in the quantized feedback system.

In time domain, the state trajectory of $z(t)$ for a k-level limit cycle can be expressed as

$$z(t) = \begin{cases} \mathrm{e}^{A(t)}z(0) + \int_0^t \mathrm{e}^{A(t-\tau)}B\Delta d\tau, 0 < t < \tau_1 \\ \mathrm{e}^{A(t-\tau_1)}z(\tau_1) + \int_{\tau_1}^t \mathrm{e}^{A(t-\tau)}B2\Delta d\tau, \tau_1 < t < \tau_2 \\ \vdots \\ \mathrm{e}^{A(t-\tau_{k'-1})}z(\tau_{k'-1}) + \int_{\tau_{k'-1}}^t \mathrm{e}^{A(t-\tau)}Bk'\Delta d\tau, \tau_{k'-1} < t < \tau_{k'} \\ \mathrm{e}^{A(t-\tau_{k'})}z(\tau_{k'}) + \int_{\tau_{k'}}^t \mathrm{e}^{A(t-\tau)}B(-(k'-1)\Delta)d\tau, \tau_{k'} < t < \tau_{k'+1} \\ \vdots \\ \mathrm{e}^{A(t-\tau_{2k'-2})}z(\tau_{2k'-2}) + \int_{\tau_{2k'-2}}^t \mathrm{e}^{A(t-\tau)}B(-\Delta)d\tau, \tau_{2k'-2} < t < \tau_{2k'-1} \end{cases} \tag{4.5}$$

where τ_i s are the time instants when the state trajectory traverses the switching planes. In our study, we denote the time instants where periodic switching occur as $(0, \tau_1, \tau_2, \ldots, \tau_{2k'-1}, T/2)$ where $k' = 0.5(k-1)$, k is the number of quantization levels and $T/2$ is the half-period of the symmetrical limit cycle.

Example 4.1. Consider an example of a limit cycle for a 5-level quantizer and a plant with transfer function $G(s) = \frac{6.5}{s^3+s^2+2s+4}$. For the 5-level quantizer($k = 5, \Delta = 5, M = 10$), the switching planes occur at $(-1.5\Delta, -0.5\Delta, 0.5\Delta, 1.5\Delta)$ and the switching time instants, $(0, \tau_1, ..., \tau_j, T/2), j \leq 3$ are as shown in Figure 4.2, where $t = 0$ is relative to a positive switching edge.

The existence of self oscillations will be determined by extending the periodic switching conditions similar to those in Chapter 2. The stability of the limit cycles will be analysed through the Jacobian of the Poincaré map. By further examining the limits on the eigenvalues of the Jacobian, limits on the quantization step size can be obtained. Thus, numerical bounds on the quantization step size where

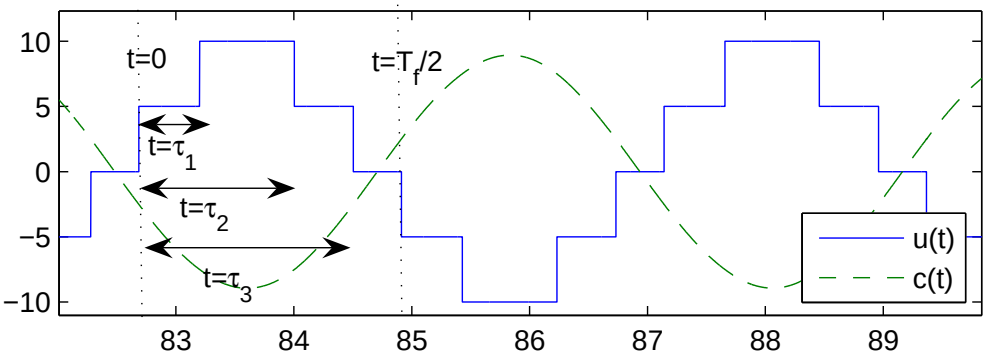

Fig. 4.2. 5-level limit cycle.

stable self oscillations exist, can be determined. In the next section, the necessary conditions for the existence of limit cycles and the stability of the limit cycles under high quantization resolution are shown.

4.3 Analysis

In this section, the extension of the periodic switching conditions in Chapter 2 will be presented, followed by the analysis on the limit cycle stability. Lastly, results on special cases will be shown.

4.3.1 Limit Cycles

The necessary conditions for limit cycles will be examined in this section. The derivation of the limit cycle solution will be presented.

Proposition 4.1. *Consider the quantized feedback system given in (4.1) and (4.2). Assume that there exists a symmetric k-level periodic solution with switching times*

$(\tau_1, \tau_2, \ldots \tau_{2k'-1})$ and period T where $k' = 0.5(k-1)$. An extension of the necessary conditions in (2.8) leads to the following.

$$\begin{aligned} Cz(\tau_i) &= Ce^{A(\tau_j-\tau_i)}z(\tau_i) + C\int_{\tau_i}^{\tau_j} e^{A(t-\tau)}Bw\Delta d\tau = -(w-0.5)\Delta \quad (4.6) \\ Cz(T/2) &= Ce^{A(T/2-\tau_{2k'-1})}z(\tau_{2k'-1}) = 0.5\Delta \end{aligned}$$

where $\tau_0 = 0$, $i = j-1$, $j = 1, 2, \ldots, 2k'-1$, $w = k - |v|$ and $v = -k+1, -k+2, \ldots, k-2, k-1$.

Additionally,

$$\begin{aligned} \frac{\partial Cz(t)}{\partial t}|_{t=\tau_p} &< 0 \\ \frac{\partial Cz(t)}{\partial t}|_{t=\tau_q} &> 0 \\ \frac{\partial Cz(t)}{\partial t}|_{t=\tau_{T/2}} &> 0 \end{aligned} \quad (4.7)$$

where $p = 1, 2, \ldots, k'-1$ and $q = k', k'+1, \ldots, 2k'-1$.

Furthermore, the periodic solution is obtained with the initial condition

$$z(0) = -z(T/2) \quad (4.8)$$

Proof. The proof is similar to that in Proposition 2.1 and equations (4.6)-(4.8) is equivalent to the necessary conditions in Proposition 2.1. □

Remark 4.1. Note that the Jacobian of the Poincaré map, $J = \frac{\partial Cz(t)}{\partial t}|_{t=\tau_{T/2}}$ and (4.7) can be verified from Figure 4.2 where the derivatives at the switching instants satisfy (4.7).

Rearranging the equations in (4.6) and (4.7),

$$Cz(\tau_i) + (w - 0.5)\Delta = 0 \tag{4.9}$$

$$Cz(T/2) - 0.5\Delta = 0 \tag{4.10}$$

The solution of (4.9) is $(\tau_1, \tau_2, \ldots, \tau_{2k'-1}, T/2, z_m^0)$ where z_m^0 is the state at the m-th switching point and $m = 0, 1, 2, \ldots, 2k'-1$. Denoting the system of nonlinear equations (4.9) by F,

$$F(b) = 0 \tag{4.11}$$

where $b = [\tau_1; \tau_2; \ldots; \tau_{2k'-1}; T, z_m^0]$.

By the inverse-free Newton's Method, let $F_1 = \frac{1}{2}F^T F$ and denote $J_1 = F^T J$ where J is the jacobian $\partial F/\partial b$. By the updating algorithm,

$$b_n = b_{n-1} - F_1 \frac{J_1}{\|J_1\|^2},$$

b_n can be iteratively updated until the error $b_n - b_{n-1}$ converges to zero. The effectiveness of this method is verified by the example below.

Example 4.2. Consider the plant with transfer function, $G(s) = \frac{6.5}{s^3+4s^2+2s+1}$ and a 3-level quantizer where $M = \Delta = 5$ in closed loop feedback. In the absence of the quantizer, the plant is asymptotically stable under unity feedback gain. With the 3-level quantizer, a limit cycle of 1 step with $(\tau_1, T) = (1.5302, 4.4646)$ is obtained,

as shown in Figure 4.3. By the inverse-free Newton's method, after 1500 iterations,

$$J = \begin{bmatrix} -14.0990 & 0 & 7.0259 & 1.5717 \\ -23.4021 & 9.9244 & 7.8565 & 1.9069 \\ -1.4069 & -0.7110 & 1.0406 & 0.0353 \\ 1.7068 & -0.7961 & -0.3640 & 0.8996 \end{bmatrix} \tag{4.12}$$

$$b_{1500} - b_{1499} = 10^{-4} \begin{bmatrix} -0.1115 \\ -0.0337 \\ -0.0392 \\ -0.0090 \end{bmatrix} \tag{4.13}$$

and $(\tau_1, T, z_2(0), z_3(0)) = (1.5306, 4.4646, -.0117, -0.4832)$. Note that in the Jacobian of the solution, $J_{11}, J_{22}, J_{33}, J_{44}$ correspond to the gradient at the switching instants. It is evident that the solution satisfies all the necessary conditions in (4.7) as $J_{11} < 0, J_{22} > 0, J_{33} > 0, J_{44} > 0$.

In the next section, the stability of the limit cycles will be studied.

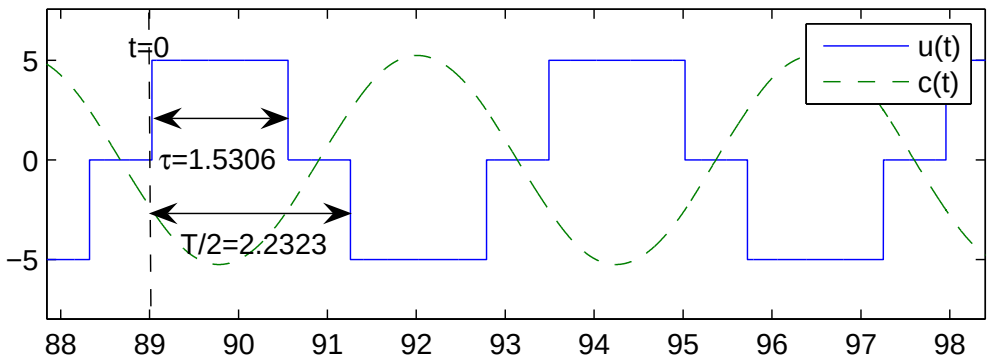

Fig. 4.3. 3-level limit cycle.

4.3.2 Stability of Limit Cycles

In this section, the local stability of the limit cycle with the computed switching times and period, will be checked by studying the effect of perturbations at each switching time instant. The Jacobian of the Poincaré map is used for this purpose, similar to (K.J.Åström, 1995; H. Olsson, 2001; Mario di Bernardo, 2001). For a k-level odd symmetric limit cycle, the switching time instants are $(0, \tau_1, \tau_2, \ldots, \tau_{2k'-1}, T/2)$ where $k' = 0.5(k-1)$. It will be shown in the proof that if these $2k'$ switching instants are analysed, the eigenvalues of $2k'$ Jacobians resulting from the Poincaré maps originating from each switching time instant, is required to be inside the unit disk. A further examination reveals that the Jacobians have the same eigenvalues and it suffices to examine the eigenvalue of one Jacobian, as shown in the Proposition below.

Proposition 4.2 (Local stability)**.** *Consider the system with closed loop quantized feedback in Figure 4.1. Assume that there is a k-level symmetric periodic solution. Let z_0^m be the state of the system when it traverses each switching plane and $w\Delta$ be the corresponding quantizer output value where $m = 0, 1, 2, \ldots, 2k' - 1$ and $w = k - |v|$ and $v = -k+1, -k+2, \ldots, k-2, k-1$.. The corresponding Jacobian of the Poincaré map is given by*

$$W = \prod_{i=1}^{k-1} W_i \tag{4.14}$$

where

$$W_i = (I - \frac{\nu_i C}{C\nu_i})\Phi_i \tag{4.15}$$

and $\Phi_i = \mathrm{e}^{A(\tau_i - \tau_{i-1})}$, $\tau_0 = 0$, $\nu_i = Aa_i + Bw\Delta$. *The limit cycle is locally stable if and only if all eigenvalues of* W *are inside the unit disk.*

Proof. Consider the trajectory resulting from the perturbed initial condition $z(0) = a_0 + \delta a_0$. The perturbation is chosen such that it satisfies the switching condition

$$C(a_0 + \delta a_0) = -0.5\Delta. \tag{4.16}$$

The perturbed solution is

$$z(t) = \mathrm{e}^{At}(a_0 + \delta a_0) + \int_0^t \mathrm{e}^{A(t-s)} Bu(s)ds. \tag{4.17}$$

Assume that the solution reaches the first switching plane at time $\tau_1 + \delta\tau_1$. Hence,

$$\begin{aligned} z(\tau_1 + \delta\tau_1) &= \mathrm{e}^{A(\tau_1+\delta\tau_1)}(a_0 + \delta a_0) - \int_0^{\tau_1+\delta\tau_1} \mathrm{e}^{A(\tau_1+\delta\tau_1-s)} dsB\Delta \qquad (4.18)\\ &= \Phi_1(I + A\delta\tau_1)(a_0 + \delta a_0) + (I + A\delta\tau_1)(\int_0^{\tau_1} \mathrm{e}^{Aw} dwB\Delta + B\Delta\delta\tau_1)\\ &= z(\tau_1) + \Phi_1\delta a_0 + (Az(\tau_1) + B\Delta)\delta\tau_1 + O(\delta^2)\\ &= a_1 + \Phi_1\delta a_0 + \nu_1\delta\tau_1 + O(\delta^2) \end{aligned}$$

where $z(\tau_1) = a_1$, $\Phi_1 = \mathrm{e}^{A\tau_1}$ and $\nu_1 = Aa_1 + B\Delta$. For $Ca_1 = Cz(\tau_1 + \delta\tau_1)$, we get

$$\delta\tau_1 = -\frac{C\Phi_1}{C\nu_1}\delta a_0 + O(\delta^2)$$

.

Inserting this in (4.18) gives

$$z(\tau_1 + \delta\tau_1) = a_1 + (I - \frac{\nu_1 C}{C\nu_1})\Phi_1\delta a_0 + O(\delta^2) \tag{4.19}$$

The perturbation at time $\tau_1 + \delta\tau_1$ is thus given by $\delta a_1 = (I - \frac{\nu_1 C}{C\nu_1})\Phi_1\delta a_0 + O(\delta^2)$.

In the same way, we can study how the perturbation δa_1 of a_1 affects the solution at time $\tau_1 + \delta\tau_1 + \tau_2 + \delta\tau_2$. We get

$$\begin{aligned} z(\tau_1 + \delta\tau_1 + \tau_2 + \delta\tau_2) &= a_2 + (I - \frac{\nu_2 C}{C\nu_2})\Phi_2 \delta a_1 + O(\delta^2) \quad (4.20) \\ &= a_2 + (I - \frac{\nu_2 C}{C\nu_2})\Phi_2 1 (I - \frac{\nu_1 C}{C\nu_1})\Phi_1 \delta a_0 + O(\delta^2). \quad (4.21) \end{aligned}$$

We follow through the same analysis till time $\tau_1+\delta\tau_1+\tau_2+\delta\tau_2+\cdots+T/2+\delta T/2$. Finally,

$$z(\tau_1+\delta\tau_1+\tau_2+\delta\tau_2+\cdots+T/2+\delta T/2) = -a_0+\prod_{i=1}^{k-1}(I-\frac{\nu_i C}{C\nu_i})\Phi_i \delta a_0+O(\delta^2). \quad (4.22)$$

Thus, the Jacobian of the Poincaré map is given by (4.14).

Next, consider the trajectory resulting from the perturbed initial condition $z(\tau_1) = a_1 + \delta a_1$. We follow through the same analysis and the jacobian of the Poincaré map is

$$W = (\prod_{i=2}^{k-1} W_i)W_1 \quad (4.23)$$

where

$$W_i = (I - \frac{\nu_i C}{C\nu_i})\Phi_i \quad (4.24)$$

and $\Phi_i = \mathrm{e}^{A(\tau_i - \tau_{i-1})}$, $\tau_0 = 0$, $\nu_i = Aa_i + Bw\Delta$.

If we let $Q = W_1(\prod_{i=2}^{k-1} W_i)$ and $P = (\prod_{i=2}^{k-1} W_i)W_1$, left-multiply Q by Φ_1^{-1} and right-multiply Q by Φ_{k-1}^{-1},

$$\Phi_1^{-1} Q \Phi_{k-1}^{-1} = (I - \Phi_1^{-1}\frac{\nu_1 C}{C\nu_1}\Phi_1)(\prod_{i=2}^{k-2} W_i)(I - \frac{\nu_{k-1} C}{C\nu_{k-1}}) \quad (4.25)$$

Left-multiply P by $(I - \Phi_1^{-1}\frac{\nu_1 C}{C\nu_1}\Phi_1)$,

$$\begin{aligned}(I - \Phi_1^{-1}\frac{\nu_1 C}{C\nu_1}\Phi_1)P &= (I - \Phi_1^{-1}\frac{\nu_1 C}{C\nu_1}\Phi_1)(\prod_{i=2}^{k-1} W_i)W_1 \\ &= \Phi_1^{-1}Q\Phi_{k-1}^{-1}\Phi_{k-1}W_1 \\ &= \Phi_1^{-1}Q\Phi_1(I - \Phi_1^{-1}\frac{\nu_1 C}{C\nu_1}\Phi_1)\end{aligned}$$

$$\Rightarrow (I - \Phi_1^{-1}\frac{\nu_1 C}{C\nu_1}\Phi_1)P = \Phi_1^{-1}Q\Phi_1(I - \Phi_1^{-1}\frac{\nu_1 C}{C\nu_1}\Phi_1)$$

Let $S = (I - \Phi_1^{-1}\frac{\nu_1 C}{C\nu_1}\Phi_1)$ and $Q' = \Phi_1^{-1}Q\Phi_1$,

$$SP = Q'S$$

$$SPS^{-1} = Q'$$

As $Q' = \Phi_1^{-1}Q\Phi_1$ and Φ_1 is always invertible, the eigenvalues of Q' and Q have the same eigenvalues. This further implies that P and Q also have the same eigenvalues.

We have now shown that $(\prod_{i=2}^{k-1} W_i)W_1$ has the same eigenvalues as $(\prod_{i=1}^{k-1} W_i)$. By following the same steps for perturbations at the other switching instants, we can derive a Jacobian for each switching instant. Starting from perturbation at $z(\tau_1)$, the corresponding Jacobian will be $(\prod_{i=3}^{k-1} W_i)W_1W_2$. Similar to the proof above, the eigenvalues of $(\prod_{i=3}^{k-1} W_i)W_1W_2$ is the same as in $(\prod_{i=1}^{k-1} W_i)$. This applies for the perturbations at all other switching instants. Thus, we find that the eigenvalues of all the jacobians are similar and hence the requirement for the eigenvalues of one Jacobian to be in the unit circle suffices. This completes the proof. □

Remark 4.2. The local stability of each traversal point of the limit cycle is checked in the proposition. Note that without the computed switching times and period, the jacobian W cannot be evaluated.

Remark 4.3. One of the eigenvalues of the jacobian is 0 as C is a left eigenvector of $(I - \frac{\nu_i C}{C\nu_i})$.

In Equation (4.23), ν_i is a function of the quantization step size, Δ. Thus, the Jacobian J is also a function of Δ. Thus, the limits on the eigenvalues of the Jacobian matrix, $|\Lambda(W) < 1|$ implies limits on the quantization step size. However, given the complexity of the solution of the Jacobian for high orders plants, explicit solutions for the limits on the quantization step size cannot be determined for all systems. Hence, the limits on Δ are demonstrated on a simple second order system, as shown in Proposition 4.3.

Example 4.3. Consider the same plant in example 4.2 with $\Delta = 2.5$ and $M = 5$. A 2-step limit cycle solution

$$(\tau_1, \tau_2, \tau_3, T, z_1(0), z_2(0), z_3(0)) = (0.5347, 1.2953, 1.8123, 4.4532, 0.1918, 0.9040, -0.4305)$$

is obtained by solving (4.11). This is verified in simulation, as shown in Figure 4.5 and 4.4. The states $z_1(0), z_2(0)$ and $z_3(0)$ are verified in Figure (4.8) where $z_{0i}(m)$ represents the mth zero-crossings and $i = 1, 2, 3$. The solution is locally stable by Proposition 4.2. The eigenvalues of (4.14) are $0.0101606, 0.3296, 0$ which are in the unit disk.

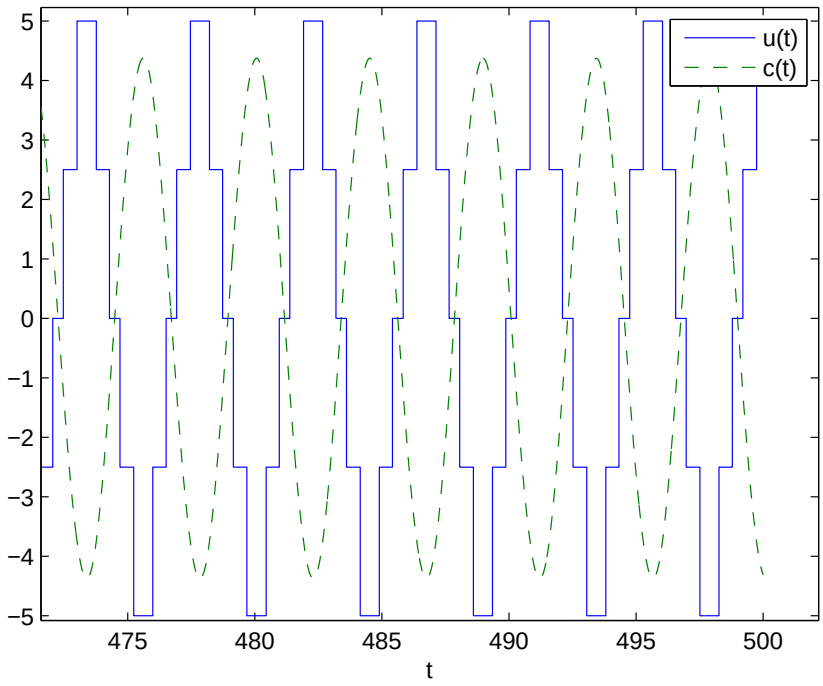

Fig. 4.4. 2 step limit cycle with $\Delta = 2.5$.

By solving (4.11), we also found that the quantizer with a step size of $\Delta = 0.05$ produced a 2-step limit cycle

$$(\tau_1, \tau_2, \tau_3, T, z_1(0), z_2(0), z_3(0)) =$$

$$(0.5330, 1.2984, 1.8136, 4.454, 0.003836, 0.01795, -0.0085).$$

By Proposition 4.2, we find that the eigenvalues are $0.0102, 0.3304, 0$, which are within the unit disk and the limit cycle is locally stable. This has been verified in simulation using a 41-level quantizer.

For $\Delta = 5/20 = 0.25$, M=5 and k=41, the quantizer output $u(t)$ converged to a 2-step limit cycle of amplitude $2 \times 0.25 = 0.5$, as shown in Figure 4.6. If we

further decrease the step size Δ to 0.05, M=5 and k=201, the quantizer output again converged to a 2-step limit cycle of amplitude $2 \times 0.05 = 0.1$, as shown in Figure 4.7. As the quantization step size decreased from 0.25 to 0.05, the quantizer output amplitude has decreased accordingly but the 2 step limit cycle remains at steady state.

In the next section, results for special cases on first and second order systems are presented. For first order systems, the conditions where self oscillations cannot occur are determined. In second order systems, the limits on the quantization step size for stable self oscillations are identified.

4.3.3 Special Cases

A. First order plants without delay

For first order plants without delay, it is generally well known that first order plants do not self oscillate under relay feedback. It can be checked that a first order non-delayed plant does not self oscillate when placed in closed loop with a quantizer as follows.

From (4.5), we can derive that

$$\begin{aligned} Cz(T/2) &= Ce^{A(T/2-\tau_{2k'-1})}z(\tau_{2k'-1}) \\ &= e^{A(T/2-\tau_{2k'-1})}Cz(\tau_{2k'-1}) \end{aligned}$$

Applying the conditions in (4.6),

$$0.5\Delta = e^{A(T/2-\tau_{2k'-1})}(-0.5\Delta) \tag{4.26}$$

As $e^{A(T/2-\tau_{2k'-1})} > 0$, we know that (4.26) cannot be possible. Thus, self oscillation cannot occur with first order plants without delay.

B. First order plants with delay

In first order systems with a 1-step quantizer and delay where $0 < L < \tau$ and $0 < \tau < T/2$, the necessary conditions (4.6) and (4.8) are satisfied when $T/2 < L + \tau < T$ and $T > 2L + \tau$. This is shown as follows.

Consider two cases: $0 < L + \tau < T/2$ and $T/2 < L + \tau < T$.

Case 1: $0 < L + \tau < T/2$

$$Cz(\tau) = Ce^{A\tau}z(0) - C(I - e^{A(\tau-L)})A^{-1}B\Delta \tag{4.27}$$

$$= -0.5e^{A\tau}\Delta - C(I - e^{A(\tau-L)})A^{-1}B\Delta \tag{4.28}$$

For a limit cycle to exist, $Cz(\tau) = -0.5\Delta$. As the right hand side of (4.27) is positive, no limit cycle is possible for $0 < L + \tau < T/2$.

Case 2: $T/2 < L + \tau < T$

$$Cz(\tau) = Ce^{A\tau}z(0) - Ce^{A(T/2-L)}(e^{A(\tau+L-T/2)} - I)A^{-1}B\Delta \tag{4.29}$$

$$= -0.5e^{A\tau}\Delta - Ce^{A(T/2-L)}(e^{A(\tau+L-T/2)} - I)A^{-1}B\Delta \tag{4.30}$$

The right hand side in (4.29) is negative and the switching condition $Cz(\tau) = -0.5\Delta$ may be satisfied. Next, the switching condition at $t = T/2$ is examined.

$$Cz(T/2) = Ce^{A\tau}z(0) + Ce^{A(L)}(e^{A(T-2L-\tau)} - I)A^{-1}B\Delta \tag{4.31}$$

If the switching condition at $t = T/2$ is satisfied,

$$0.5(I + e^{A\tau})\Delta = Ce^{A(L)}(e^{A(T-2L-\tau)} - I)A^{-1}B\Delta \tag{4.32}$$

$$e^{A(T-2L-\tau)} - I < 0 \tag{4.33}$$

$$T > 2L + \tau \tag{4.34}$$

The necessary conditions at $t = \tau$ and $t = T/2$ have been examined. By Proposition 4.1, $W = 0$ for first order plants. The eigenvalue $\lambda(W)$ is within the unit disk. Thus, the limit cycle for first order plants is also locally stable by Proposition 4.1. Hence, for first order plants with delay, a limit cycle can exist for $T/2 < L + \tau < T$ and $T > 2L + \tau$.

C. Second order plants

For second order plants with state space representation,$A = [0\ 1;\ -\lambda_1\lambda_2\ (\lambda_1 + \lambda_2)]$, $B = [0\ 1]^T$ and $C = [c\ 0]$ where $\lambda_1 < \lambda_2 < 0$ are the roots of the plant, limit cycles may not always exist. For second order systems with delay, a limit cycle may exist if the necessary conditions in (4.6) and (4.7) are satisfied. As previously mentioned in Section 4.3.2, the limits on the eigenvalues of the Jacobian matrix, $|\lambda(W)| < 1$ in Proposition 4.2 allows us to calculate the limits on the quantization step size. This is demonstrated on a second order system with a 3-level quantizer, as shown in the proposition below.

Proposition 4.3. *For a second order plant in negative feedback with a* 3*-level*

quantizer, the limit cycle with solution set (τ, T, L) *is locally stable if and only if*

$$\Delta > \max_{z_2(0)\in R}\{\Delta_1\}, \tag{4.35}$$

$$\max_{z_2(0)\in R}\{\Delta_2\} < \Delta < \min_{z_2(0)\in R}\{\Delta_3\}, \tag{4.36}$$

$$\Delta > \max_{z_2(0)\in R}\{\Delta_3, \Delta_4\} \tag{4.37}$$

or

$$\Delta < \min_{z_2(0)\in R}\{\Delta_1\}, \tag{4.38}$$

$$\max_{z_2(0)\in R}\{\Delta_4\} < \Delta < \min_{z_2(0)\in R}\{\Delta_3\}, \tag{4.39}$$

$$\Delta > \max_{z_2(0)\in R}\{\Delta_3\} \tag{4.40}$$

where

$$\Delta_1 = \frac{-2z_2(0)(\lambda_1 \mathrm{e}^{\lambda_1 L+0.5\lambda_2 T+2\lambda_1\tau}-\lambda_2 \mathrm{e}^{\lambda_2 L+0.5\lambda_1 T+2\lambda_2\tau})}{\lambda_1\lambda_2(\mathrm{e}^{\lambda_2 L+0.5\lambda_1 T+2\lambda_2\tau}-\mathrm{e}^{\lambda_1 L+0.5\lambda_2 T+2\lambda_1\tau})+2\mathrm{e}^{0.5(\lambda_1+\lambda_2)T}(\mathrm{e}^{\lambda_1\tau}-\mathrm{e}^{\lambda_2\tau})} \tag{4.41}$$

$$\Delta_2 = \frac{-2z_2(0)(\lambda_1 \mathrm{e}^{\lambda_1 L+0.5\lambda_2 T+2\lambda_1\tau}-\lambda_2 \mathrm{e}^{0.5\lambda_1 T+\lambda_2 L+2\lambda_2\tau})}{\lambda_1\lambda_2(\mathrm{e}^{\lambda_2 L+\lambda_1 T+2\lambda_2\tau}-\mathrm{e}^{\lambda_1 L+\lambda_2 T+2\lambda_1\tau}+\mathrm{e}^{\lambda_2 L+0.5\lambda_1 T+2\lambda_2\tau}-\mathrm{e}^{\lambda_1 L+0.5\lambda_2 T+2\lambda_1\tau})+2\mathrm{e}^{0.5(\lambda_1+\lambda_2)T}(\mathrm{e}^{\lambda_1\tau}-\mathrm{e}^{\lambda_2\tau})} \tag{4.42}$$

$$\Delta_3 = \frac{2z_2(0)}{\lambda_1\lambda_2} \tag{4.43}$$

$$\Delta_4 = \frac{2z_2(0)(\lambda_1 \mathrm{e}^{\lambda_1 L+0.5\lambda_2 T+2\lambda_1\tau}-\lambda_2 \mathrm{e}^{0.5\lambda_1 T+\lambda_2 L+2\lambda_2\tau}+\lambda_2 \mathrm{e}^{\lambda_1 T+\lambda_2 L+2\lambda_2\tau}-\lambda_1 \mathrm{e}^{\lambda_1 L+\lambda_2 T+2\lambda_1\tau})}{\lambda_1\lambda_2(\mathrm{e}^{\lambda_2 L+\lambda_1 T+2\lambda_2\tau}-\mathrm{e}^{\lambda_1 L+\lambda_2 T+2\lambda_1\tau}-\mathrm{e}^{\lambda_2 L+0.5\lambda_1 T+2\lambda_2\tau}+\mathrm{e}^{\lambda_1 L+0.5\lambda_2 T+2\lambda_1\tau})-2\mathrm{e}^{0.5(\lambda_1+\lambda_2)T}(\mathrm{e}^{\lambda_1\tau}-\mathrm{e}^{\lambda_2\tau})} \tag{4.44}$$

where $\lambda_1\lambda_2(\mathrm{e}^{\lambda_2 L+0.5\lambda_1 T+2\lambda_2\tau} - \mathrm{e}^{\lambda_1 L+0.5\lambda_2 T+2\lambda_1\tau}) + 2\mathrm{e}^{0.5(\lambda_1+\lambda_2)T}(\mathrm{e}^{\lambda_1\tau} - \mathrm{e}^{\lambda_2\tau}) > 0.$

Proof. By expanding the limits on the eigenvalues of the Jacobian matrix, $|\lambda(W)| < 1$, the results (4.35) to (4.40) are obtained. (4.35)-(4.37) and (4.38)-(4.40) are derived corresponding to $0 < \lambda < 1$ and $-1 < \lambda < 0$ respectively. □

From Proposition 4.3, if quantization step size $\Delta > \max\{\Delta_1\,\Delta_2, \Delta_3, \Delta_4\}$, the limit cycle is locally stable.

Consider an example, $A = \begin{bmatrix} 0 & 1 \\ -0.5 & -1 \end{bmatrix}$, $B = \begin{bmatrix} 0 \\ 1 \end{bmatrix}$, $C = \begin{bmatrix} 6.5 & 0 \end{bmatrix}$, $L = 1$. For this plant at $\Delta = 0.0005$, the limit cycle $(\tau, T, z_1(0), z_2(0)) = (2.819, 3.002, -0.0000387, -0.0004985)$ exists. By Proposition 4.3, the limit cycle $(\tau, T) = (2.819, 3.002)$ is stable for $0.000233131 < \Delta < 0.0001849, 0.00849123 < \Delta < 0.0132733, \Delta > 0.0132733$. This further confirms the existence of limit cycles at $\Delta = 0.0005$. The limit cycle is shown in Figure 4.9(a). The states $z_1(0), z_2(0)$ are also verified in 4.9(b) where $z_0i(m)$ represents the mth zero-crossings and $i = 1, 2$.

In this section, the stability of the limit cycle has been investigated. The limit cycle stability can be determined by evaluating the magnitude of the eigenvalues of the Jacobian W. In a particular example, it was found that the quantizer output converged to a 2-step limit cycle of a small amplitude at small quantization step sizes. Note that by increasing quantization resolution, a 2-step limit cycle with a small amplitude was still obtained. The special cases examined, reveals the conditions required for limit cycles to exist. For a second order plant with a 3-level quantizer, the bounds of the quantization step size for stable limit cycles have been identified. For higher order plants, explicit expressions for the bounds on the quantization step size cannot be identified due to the numerical difficulties

in solving for Δ.

4.4 Conclusions

In this chapter, the necessary conditions for the existence of limit cycles with various levels and their stability have been examined in continuous time. A study of the local stability of the limit cycles was performed by analysing the eigenvalues of the Jacobian of the Poincaré map for each switching instant. It was shown that the Jacobians for each switching instant have the same eigenvalues and it suffices to analyse only one Jacobian. At high quantization resolution, the system with the uniform quantizer may converge exponentially to a limit cycle whose amplitude is related to Δ. The stability of the limit cycle can be identified by evaluating the magnitude of the eigenvalues of the Jacobian W of the Poincaré map. It was found that stable limit cycles can still exist under high quantization resolution. In a particular example, the quantizer output converged to a 2-step limit cycle of a small amplitude at small quantization step sizes. The special cases examined, reveal the conditions required for limit cycles to exist. For a second order plant with a 3-level quantizer, the bounds on the quantization resolution for which limit cycles exist, are shown.

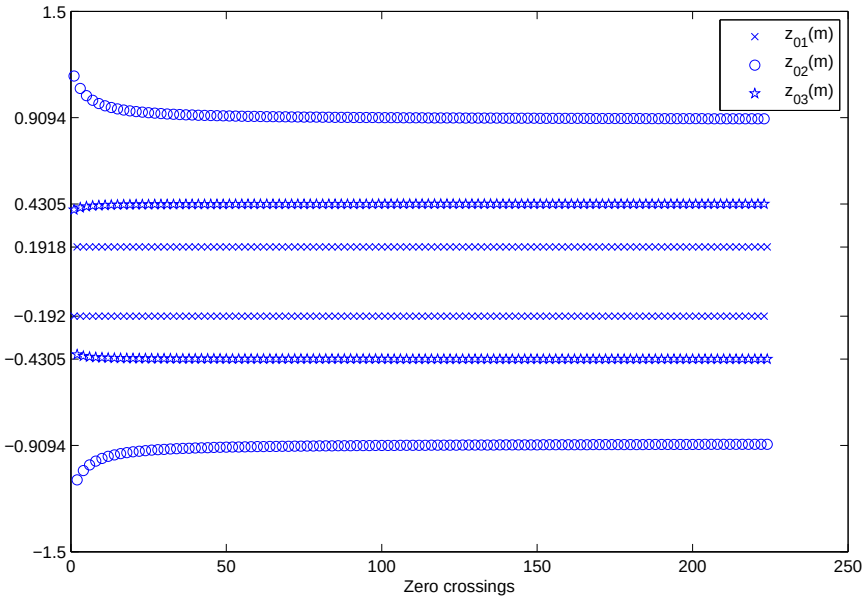

Fig. 4.5. States of 2 step limit cycle with $\Delta = 2.5$.

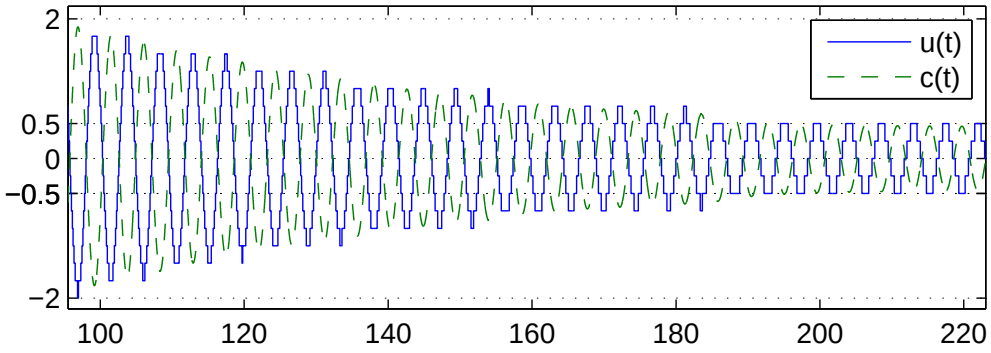

Fig. 4.6. 2 step limit cycle with $\Delta = 0.25$.

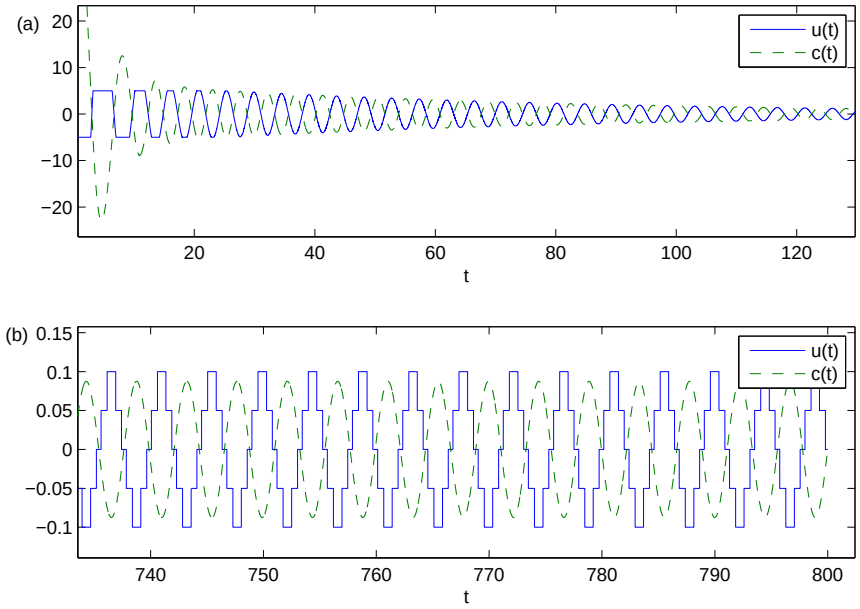

Fig. 4.7. 2 step limit cycle with $\Delta = 0.05$.

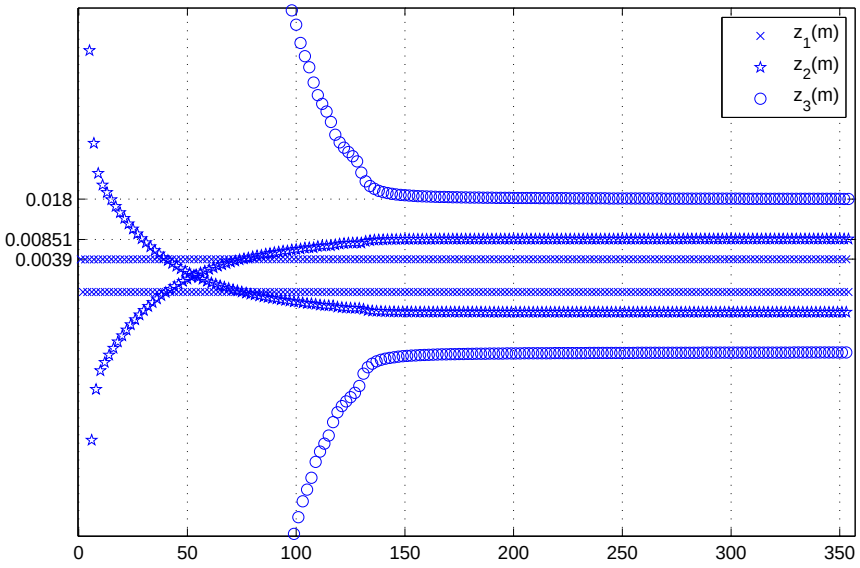

Fig. 4.8. States of 2 step limit cycle with $\Delta = 0.05$.

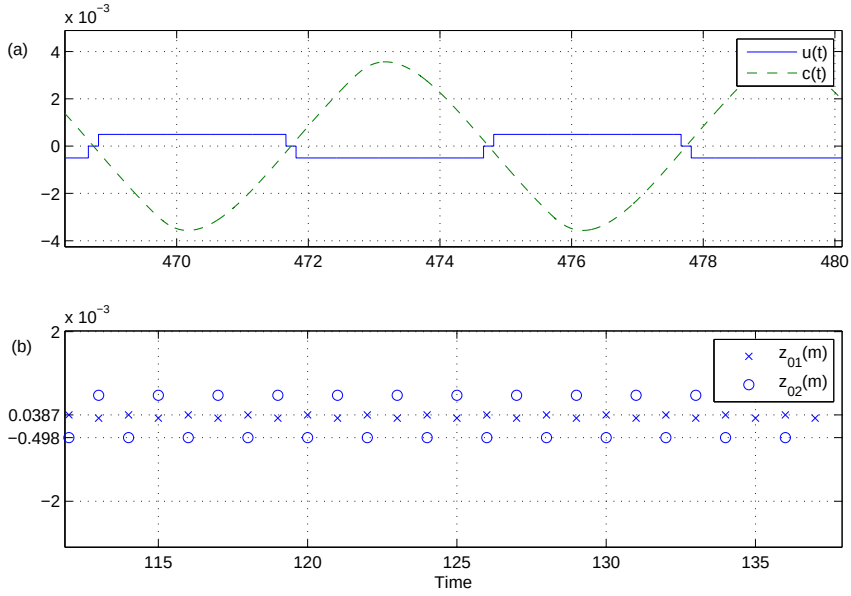

Fig. 4.9. (a) 1 step limit cycle with $\Delta = 0.0005$. (b)States of 1 step limit cycle with $\Delta = 0.0005$.

Chapter 5

Conclusions

5.1 Main Findings

In this thesis, several new results are obtained. Briefly, the results are summarised as follows:

A. Forced and Subharmonic Oscillations under Relay Feedback

The conditions for stable FO and SO to occur in a sinusoidally forced single loop RFS were examined. It was found that the external forcing signal requires a minimum amplitude, R_{min}, for either FO or SO to occur. A combination of a graphical approach using the Tsypkin Locus and a numerical approach was used to determine this R_{min}. The main contribution of this chapter lies in the discovery of the fundamental difference between FO and SO. FO is possible for any frequency of the external forcing signal as long as its amplitude was sufficiently large. This was however not the case for SO. A complex relationship between frequency, amplitude and ν exists for SO. Specifically, not all forcing signals can drive the RFS at

any order ν even if the amplitude of the external signal is large. The ranges of frequencies where SO of certain orders can be obtained were derived. Results for FOPDT plants were completely given. Other behaviours for higher order plants were also presented.

B. Design of Amplitude Reduction Dithers in Relay Feedback Systems

Using the idea from forced oscillations, the potential of using a dither in arbitrarily reducing inherent system oscillations has been illustrated. The bound on the dither period, T_f^* was determined and shown to be independent of the dither shape. The analysis is exact and results can be obtained from the generalized Tsypkin Loci. For first and second order real plants, it was shown that $T_f^* = \infty$ which implies that quenching can be achieved with arbitrarily small amplitudes.

C. Limit Cycles in Quantized Feedback Systems under High Quantization Resolution

In this chapter, the necessary conditions for the existence of limit cycles with various quantizer levels and their stability were examined in continuous time. A study of the local stability of the limit cycles was performed by analysing the eigenvalues of the Jacobian of the Poincare map for each switching instant. It was shown that the Jacobians for each switching instant have the same eigenvalues and it sufficed to analyse only one Jacobian. As the number of quantization level k increased, the system with the uniform quantizer converged exponentially to a limit cycle whose amplitude is related to Δ. One of the parameters that affects the stability of the limit cycle solution is the quantization step size Δ. The limits on

Δ was identified by evaluating the magnitude of the eigenvalues of the Jacobian W for a range of Δ. In a particular example, it was found that the quantizer output converged to a 2-step limit cycle of a small amplitude at small quantization step sizes. Note that by increasing quantization resolution, a 2-step limit cycle with a small amplitude was obtained. The special cases examined, revealed the conditions required for limit cycles to exist. For a second order plant with a 3-level quantizer, the effects of the quantization step size on the existence of limit cycles were examined.

5.2 Suggestions for Further Work

Some topics remain open and are recommended for future work.

A. Forced and Subharmonic oscillations for general nonlinearities

The analysis of forced and subharmonic oscillations for relay feedback systems have been analysed and presented in this proposal. A natural extension of the results in this proposal is to examine the same switching conditions for other types of nonlinear systems and to determine the exact requirements for forced and subharmonic oscillations to occur. The choice of a meaningful system for analysis is critical. The behaviours of sinusoidally forced nonlinear systems which are smooth and continuous have been widely studied but that is not for the case of non-smooth continuous systems. The reason is as follows.

For autonomous systems, we can analyse the stability of the equilibrium points

easily whereas in non-autonomous systems with an external sinusoidal forcing signal, we may only achieve boundness of solutions. The problem of stability analysis is even more difficult in non-smooth continuous systems, as the local Lipschitz condition is obviously violated. Hence, for non-smooth continuous systems, even boundness of solutions cannot be proved easily. Although it is a great challenge to try to analyse such systems but it might still be a worthwhile attempt as the bifurcation of fixed points and periodic solutions and chaos arising from such systems have received great attention in recent years.

B. Subharmonics control, Chaos control and switching bifurcations

The work on bifurcations and chaos control for nonlinear systems have been extensive. Some examples are as follows. The bifurcations and the route to chaos for an externally forced dry friction oscillator was studied in Mario di Bernardo (2003). In G. Bagni and Tesi (2004) and M. Basso and Giovanardi (2002), a central issue in bifurcations and chaos control application is addressed. In those papers, the design of controllers are proposed to ensure stable periodic motions in sinusoidally forced nonlinear systems, thereby achieving chaos control.

We have seen in this proposal that only a small amplitude is required to generate SO in the case of piecewise linear systems. Thus, they are extremely sensitive to tiny perturbations. These tiny perturbations which could exist due to noise in the environment could lead to chaotic behaviour. On the other hand, its sensitivity to perturbations could also be used to stabilise and control the system to regular and predictable dynamical behaviour like SO. One can study this behaviour for future work.

Author's Publications

[1] Loh AP, Lim LH, Fu J, Fong KF (2004). Forced and Subharmonic Oscillations in Relay Feedback Systems. *In Proceedings of the 6th IASTED International Conference on Intelligent Systems and Control (ISC 2004), Honolulu, Hawaii, USA, 2004.*

[2] Lim LH, Loh AP, Fu J (2005). Estimation of Minimum Conditions for Forced Oscillations in Relay Feedback Systems. *In 2005 International Conference on Control and Automation, 27-29 June 2005, Hungarian Academy of Science, Budapest, Hungary, 27 June 2005.*

[3] Lim LH, Loh AP (2005). Forced and Subharmonic Oscillations in Relay Feedback Systems. *Journal of Institution of Engineers, Singapore* **45**(5), pg 88-100.

[4] Lim LH, Loh AP (2006). Identification of Frequency Ranges for Subharmonic Oscillations in a Relay Feedback System. *In 2006 American Control Conference, 14-16 June 2006, Minnepolis, Minnesota, 15 June 2006, pg 3789-3794.*

[5] Lim LH, Loh AP (2008). Sinusoidal Dither in a Relay Feedback System. *In*

2008 American Control Conference, 11-13 June 2008, pg 1893-1898.

[6] Lim LH, Loh AP (2008). On Forced and Subharmonic Oscillations under Relay Feedback. *IET Control Theory Appl.* **2**(9), pg 829-840.

[7] Lim LH, Loh AP (2008). Design of Amplitude Reduction Dithers in Relay Feedback Systems. *submitted to Automatica.*

Bibliography

A. A. Pervozvanski, C. Canudas de Wit (2002). Asymptotic analysis of the dither effect in systems with friction. *Automatica* **38**(1), 102–113.

A. Gelig, A. Churilov (1998). *Stability and Oscillations of Nonlinear Pulse Modulated Systems*. Birkhauser.

Åström K J, Hägglund (1984). Automatic tuning of simple regulators with specifications on phase and amplitude margins. *Automatica*.

Atherton, D P (1982). *Nonlinear Control Engineering, Describing Analysis and Design*. Van Nostrand Reinhold.

Bernardo, Mario Di and Karl Johansson (2001). Self-oscillations and sliding in relay feedback systems: Symmetry and bifurcations. *International Journal of Bifurcation and Chaos*.

Brad Lehman, Richard M. Bass (1996). Extensions of averaging theory for power electronic systems. *IEEE Transactions on Automatic Control*.

Curry, R.E. (1970). *Estimation and Control with Quantized Measurements*. Cambridge, MA:MIT Press.

Delchamps, D.F. (1990). Stabilizing a linear system with quantized state feedback. *IEEE Trans. Automatic Control* **35**(8), 916–924.

Feigin, M.I. (1970). Doubling of the oscillation period with c-bifurcations in piecewise continuous systems. *Applied Mathematics and Mechanics* **34**, 861–869.

Feigin, M.I. (1974). On the generation of sets of subharmonic modes in a piecewise continuous system. *Prikladnaya Matematika i Mekhanika* **38**, 810–818.

Feigin, M.I. (1994). *Forced Oscillations in Systems with Discontinuous Nonlinearities*. Moscow: Nauka.

Filippov, A F (1988). *Differential equations with discontinuous righthand sides*. Boston: Kluwer Academic Publishers.

Fridman, Leonid M. (2002). Singular perturbed analysis of chattering in relay control systems. *IEEE Trans on Automatic Control*.

Fu, Minyue and Lihua Xie (2005). The sector bound approach to quantized feedback control. *IEEE Trans. Automatic Control*.

G. Bagni, M. Basso, R. Genesio and A. Tesi (2004). Synthesis of mimo controller for extending the stability range of periodic solutions in forced nonlinear systems. *Automatica* pp. 1–10.

G. Zames, N.A. Shneydor (1976). Dither in nonlinear systems. *IEEE Transactions on Automatic Control*.

G. Zames, N.A. Shneydor (1977). Structural stabilization and quenching by dither in nonlinear systems. *IEEE Transactions on Automatic Control*.

Gibson, J E (1963). *Nonlinear Automatic Control (International Student Edition)*. McGraw-Hill Book Company.

Goncalves, J.M., A. Megretshi and M.A. Dahleh (1999). Global stability of relay feedback systems. *Technical Report Preprint LIDS-P-2458, Dept. of EECS, MIT,Cambridge,MA*.

Goncalves, Jorge M. (2005). Regions of stability for limit cycle oscillations in piecewise linear systems. *IEEE Transactions on Automatic Control*.

H. Olsson, K.J.Astrom (2001). Friction generated limit cycles. *IEEE Transactions on Control Systems Technology* **9**(4), 629–636.

Hamel, B. (1949). Contribution a li¯´etude mathematique des syst'emes de r´eglage par tout-ou-rien, c.e.m.v.. *Service Technique Aeronautique*.

J.D. Reiss, M.B. Sandler (2005). A mechanism for the detection and removal of limit cycles in the operation of sigma delta modulators. In: *5th IEE International Conference on ADDA*. pp. 217–221.

J.K.-C. Chung, D.P. Atherton (1966). The determination of periodic modes in relay systems using the state space approach. *International Journal of Control*.

Johansson, Karl Henrik, Anders Rantzer and Karl Johan Astrom (1999). Fast switches in relay feedback systems. *Automatica* **35**, 539–552.

Juha Kauraniemi, Timo I. Laakso (1996). Elimination of limit cycles in a direct form delta operator filter. In: *Proceedings of EUSIPCO*. pp. 57–60.

K, Schulz D (1991). *Effects of measurement Quantization in the Feedback Loop of Discrete-Time Linear Control Systems*. PhD Thesis, Cornell University.

Kalman, R.E. (1956). Nonlinear aspects of sampled-data control systems. In: *Proc. Symp. Nonlinear Circuit Theory*.

K.J.Åström (1995). *Oscillations in systems with relay feedback in Adaptive Control, Filtering and Signal Processing*. Springer-Verlag.

Liberzon, D. (2003). Hybrid feedback stabilization of systems with quantized signals. *Automatica* **39**, 1543–1554.

Lim, L H, A P Loh and J Fu (2005). Estimation of minimum conditions for forced oscillation in relay feedback systems. In: *International Conference on Control and Automation*. pp. 1262–1267.

Lin, Chong, Qing-Guo Wang, Tong Heng Lee and James Lam (2002). Local stability of limit cycles for time-delay relay-feedback systems. *IEEE Transactions on Circuits and Systems Part I*.

Loh, A P, J Fu and W W Tan (2000). Controller design for tito systems with mode3 oscillations. In: *IEE Control 2000 Proceedings*.

Luigi Iannelli, Karl Henrik Johansson, Ulf T. Jönsson Francesco Vasca (2003*a*). Dither for smoothing relay feedback systems. *IEEE Transaction on Circuits and Systems-I: Fundamental Theory and Applications*.

Luigi Iannelli, Karl Henrik Johansson, Ulf T. Jönsson Francesco Vasca (2003*b*). Effects of dither shapes in nonsmooth feedback systems: Experimental results and theoretical insight. In: *Proceedings of the 42nd IEEE Conference on Decision and Control*. pp. 4285–4290.

Luigi Iannelli, Karl Henrik Johansson, Ulf T. Jönsson Francesco Vasca (2006). Averaging of nonsmooth systems using dither. *Automatica* **42**, 669–676.

M. Basso, R. Genesio and L. Giovanardi (2002). *Controller Synthesis for Periodically Forced Chaotic Systems*. Chaos in Circuits and Systems, G. Chen and T. Ueta (ed.), World Scientific Pub. Co., Singapore.

Marcus Rubensson, Bengt Lennartson (2000). Stability of limit cycles in hybrid systems using discrete-time lyapunov techniques. In: *Proceedings of the 39th IEEE Conference on Decision and Control*. pp. 1397–1402.

Mario di Bernardo, C.J. Budd, A.R. Champneys (2001). Unified framework for the analysis of grazing and border-collisions in piecewise-smooth systems. *Physical Review Letters* **86**(12), 2554–2556.

Mario di Bernardo, P. Kowalczyk, A. Nordmark (2003). Sliding bifurcations: a novel machanism for the sudden onset of chaos in dry-friction oscillators. *International Journal of Bifurcation and Chaos* **13**(10), 2935–2948.

Mossaheb, S (1983). Application of a method of averaging to the study of dither in non-linear systems. *International Journal of Control* **38**(3), 557–576.

Naumov, B N (1993). *Philosophy of Nonlinear Control Systems*. Mir Publishers.

Nordmark, A. (1991). Non-periodic motion caused by grazing incidence in impact oscillators. *Journal of Sound and Vibration* **2**, 279–297.

Piccardi, Carlo (1994). Bifurcations of limit cycles in periodically forced nonlinear systems: The harmonic balance approach. *IEEE Transactions on Circuits and Systems Part I*.

Q.-G. Wang, T.H. Lee, C. Lin (2003). *Relay Feedback: Analysis, Identification and Control*. Verlag London: Springer.

R.K. Miller, A.N. Michel and J.A. Farrel (1989). Quantizer effects on steady state error specifications of digital control systems. *IEEE Trans. Automatic Control* **14**(6), 651–654.

R.W. Brockett, D. Liberzon (2000). Quantized feedback stabilization of linear systems. *IEEE Transactions on Automatic Control* **45**(7), 1279–1289.

Taylor, James H. (2000). *Electrical and Electronics Engineering Encyclopedia, Supplement 1*. John Wiley & Sons, Inc.

Toshimitsu U, Kazumasa H (1983). Chaos in non-linear sampled-data control systems. *International Journal of Control* **38**(5), 1023–1033.

Tsypkin, Y Z (1984). *Relay Control Systems*. Cambridge University Press.

Y. Levin, A. Ben-Isreal (2003). An inverse-free directional newton method for solving systems of nonlinear equations. *World Scientific, Singapore* **2**, 1447–1457.

Zames, G. and P.L. Falb (1968). Stability conditions for systems with monotone and slope restricted nonlinearities. *Siam J. Control* **6**(1), 89–108.